

Chapter 1

General Theory of Disperse Metal Electrodeposits Formation

Konstantin I. Popov and Nebojša D. Nikolić

1.1 Introduction

The most frequently used form of the cathodic polarization curve equation for flat or large spherical electrode of massive metal is given by

$$j = \frac{j_0(f_c - f_a)}{1 + \frac{j_0 f_c}{j_L}}, \quad (1.1)$$

where j , j_0 and j_L , are the current density, exchange current density, and limiting diffusion current density, respectively, and

$$f_c = 10^{\frac{\eta}{bc}}, \quad (1.2)$$

K.I. Popov (✉)

ICTM-Institute of Electrochemistry, University of Belgrade, Njegoševa 12,
P.O.B. 473,11001 Belgrade, Serbia

Faculty of Technology and Metallurgy, University of Belgrade, Karnegijeva 4,
P.O.B. 3503,11001 Belgrade, Serbia

e-mail: kosta@tmf.bg.ac.rs

N.D. Nikolić

ICTM-Institute of Electrochemistry, University of Belgrade, Njegoševa 12,
P.O.B. 473,11001 Belgrade, Serbia

e-mail: nnikolic@tmf.bg.ac.rs

$$f_a = 10^{-\frac{\eta}{b_a}}, \quad (1.3)$$

where b_c and b_a are the cathodic and anodic Tafel slopes and η is the overpotential. Equation (1.1) is modified for use in electrodeposition of metals by taking cathodic current density and overpotential as positive. Derivation of Eq. (1.1) is performed under assumption that the concentration dependence of j_0 can be neglected [1–4].

It is known [3] that electrochemical processes on microelectrodes in bulk solution can be under activation control at overpotentials which correspond to the limiting diffusion current density plateau of the macroelectrode. The cathodic limiting diffusion current density for steady-state spherical diffusion, $j_{L,Sp}$ is given by

$$j_{L,Sp} = \frac{nFDC_0}{r}, \quad (1.4)$$

and for steady-state linear diffusion, j_L , it is given by

$$j_L = \frac{nFDC_0}{\delta}, \quad (1.5)$$

where n is the number of transferred electrons, F is the Faraday constant, D and C_0 are the diffusion coefficient and bulk concentration of the depositing ion, respectively, r is the radius of the spherical microelectrode, and δ is the diffusion layer thickness of the macroelectrode. It follows from Eqs. (1.4) and (1.5) that

$$\frac{j_{L,Sp}}{j_L} = \frac{\delta}{r}. \quad (1.6)$$

An electrode around which the hydrodynamic diffusion layer can be established, being considerably lower than dimensions of it, could be considered as a macroelectrode. An electrode, mainly spherical, whose diffusion layer is equal to the radius of it, satisfying

$$\delta \gg r, \quad (1.7)$$

can be considered as a microelectrode [5].

According to Eq. (1.1) for

$$f_c \gg f_a \text{ and } \frac{j_0 f_c}{j_L} \gg 1, \quad (1.8)$$

the cathodic process on the macroelectrode enters full diffusion control, i.e.,

$$j \cong j_L. \quad (1.9)$$

Simultaneously, the cathodic current density on the spherical microelectrode, j_{Sp} , is given by

$$j_{\text{Sp}} = \frac{j_0(f_c - f_a)}{1 + \frac{j_0 f_c}{j_{L,\text{Sp}}}} \quad (1.10)$$

or, because of Eq. (1.6),

$$j_{\text{Sp}} = \frac{j_0(f_c - f_a)}{1 + \frac{j_0}{j_L} \cdot \frac{r}{\delta} \cdot f_c} \quad (1.11)$$

and, if condition (1.8) is also valid, but

$$\frac{r}{\delta} \rightarrow 0. \quad (1.12)$$

Equation (1.11) can be rewritten in the form

$$j = j_0 f_c. \quad (1.13)$$

This means that the process on the microelectrode in the bulk solution can be under complete activation control at the same overpotential at which the same process on the macroelectrode is simultaneously under full diffusion control.¹

¹ The reversible potential of a surface with radius of curvature r_{cur} would depart from that of a planar surface by the quantity $\Delta E_r = 2\sigma V / (nF r_{\text{cur}})$, where σ is the interfacial energy between metal and solution, and V is the molar volume of metal [5]. It is valid at extremely low r_{cur} , being of the order of few millivolts, and it can be neglected except in some special cases, like the stability of the shape of the tips of dendrites [5].

The different behavior of macroelectrodes and microelectrodes under the same conditions of electrodeposition causes the disperse deposits formation.

Since the paper of Barton and Bockris [5] on the growth of silver dendrites, a lot of papers, chapters, and even books, dealing with electrodeposition of disperse metals were published. The aim of this chapter is to unite the basic statements of the previous contributions in a general all-inclusive theory.

1.2 Active Microelectrodes Placed the Inside Diffusion Layer of the Active Macroelectrode

1.2.1 Basic Facts

Naturally, the microelectrodes can be placed on the macroelectrodes inside their diffusion layers. Let us consider the model of surface irregularities shown in Fig. 1.1. The electrode surface irregularities

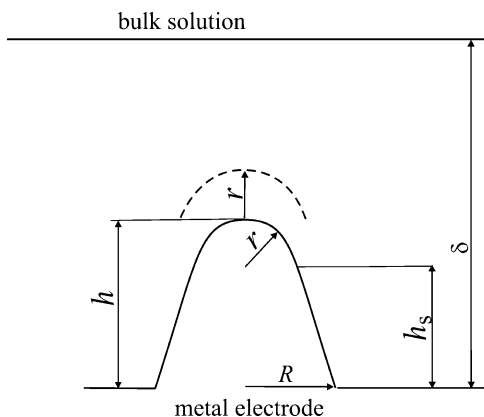


Fig. 1.1 Model of a paraboloidal surface protrusion: h is the height of the protrusion relative to the flat portion of the surface, h_s is the corresponding local side elongation, r is the radius of the protrusion tip, R is the radius of the protrusion base, δ is the thickness of the diffusion layer, and $\delta \gg h$ (Reprinted from [1] with permission from Springer and [6] with permission from Elsevier.)

are buried deep in the diffusion layer, which is characterized by a steady linear diffusion to the flat portion of the surface [1, 6, 7].

At the side of an irregularity, the limiting diffusion current density, $j_{L,S}$, is given as

$$j_{L,S} = \frac{nFDC_0}{\delta - h_s} = j_L \frac{\delta}{\delta - h_s}. \quad (1.14)$$

Obviously, this is valid if the protrusion height does not affect the outer limit of the diffusion layer and that a possible lateral diffusion flux supplying the reacting ions can be neglected. At the tip of an irregularity, the lateral flux cannot be neglected and the situation can be approximated by assuming a spherical diffusion current density, $j_{L,tip}$, given by [7]

$$j_{L,tip} = \frac{nFDC^*}{r}, \quad (1.15)$$

where C^* is the concentration of the diffusing species at a distance r from the tip, assuming that around the tip a spherical diffusion layer having a thickness equal to the radius of the protrusion tip is formed [5]. Obviously, if $R > \delta$ the spherical diffusion layer around the tips of protrusion cannot be formed and Eq. (1.16) is valid:

$$j_{L,tip} = \frac{nFDC_0}{\delta - h}. \quad (1.16)$$

If deposition to the macroelectrode is under full diffusion control, the distribution of the concentration C inside the linear diffusion layer is given by [3]

$$C = C_0 \frac{h}{\delta}, \quad (1.17)$$

where $0 \leq h \leq \delta$. Hence,

$$C^* = C_0 \frac{h + r}{\delta} \quad (1.18)$$

and

$$j_{L,\text{tip}} = j_L \left(1 + \frac{h}{r} \right) \quad (1.19)$$

because of Eqs. (1.5), (1.15), and (1.18).

The tip radius of the paraboloidal protrusion is given by [3, 5, 8]

$$r = \frac{R^2}{2h}, \quad (1.20)$$

and substitution of r from Eq. (1.20) in Eq. (1.19) gives

$$j_{L,\text{tip}} = j_L \left(1 + \frac{2h^2}{R} \right) \quad (1.21)$$

or

$$j_{L,\text{tip}} = j_L (1 + 2k^2), \quad (1.22)$$

where

$$k = \frac{h}{R}. \quad (1.23)$$

Hence for a hemispherical protrusion,

If $h = R$, $k = 1$

$$j_{L,\text{tip}} = 3j_L, \quad (1.24)$$

if $h \ll R$, $k \rightarrow 0$

$$j_{L,\text{tip}} \rightarrow j_L, \quad (1.25)$$

and if $R \ll h$, $k \rightarrow \infty$

$$j_{L,\text{tip}} \rightarrow \infty. \quad (1.26)$$

Substituting $j_{L,\text{tip}}$ from Eq. (1.22) instead of j_L in Eq. (1.1) and further rearranging gives

$$j_{\text{tip}} = \frac{j_{0,\text{tip}}(f_c - f_a)}{1 + \frac{j_{0,\text{tip}}}{j_L} \cdot \frac{1}{1+2k^2} f_c}, \quad (1.27)$$

if j_0 around the tip is $j_{0,\text{tip}}$ and if the surface energy term [3, 5] can be neglected. The current density on the tip of a protrusion, j_{tip} , is determined by k , hence by the shape of the protrusion. If $k \rightarrow 0$, $j_{\text{tip}} \rightarrow j$ (see Eq. (1.1)) and if $k \rightarrow \infty$, $j_{\text{tip}} \rightarrow j_{0,\text{tip}}(f_c - f_a) > j$. The electrochemical process on the tip of a sharp needle-like protrusion can be under pure activation control outside the diffusion layer of the macroelectrode. Inside it, the process on the tip of a protrusion is under mixed control, regardless it is under complete diffusion control on the flat part of the electrode for $k \rightarrow 0$. If $k = 1$, hence for hemispherical protrusion, j_{tip} will be somewhat larger than j , but the kind of control will not be changed. It is important to note that the current density to the tip of hemispherical protrusion does not depend on the size of it if $k = 1$. This makes a substantial difference between spherical microelectrodes in bulk solution [9] and microelectrodes inside diffusion layer of the macroelectrode [3]. In the first case the limiting diffusion current density depends strongly on the radius of the microelectrode.

1.2.2 Physical Illustration

1.2.2.1 General Observation

Activation-controlled deposition of copper produces large grains with relatively well-defined crystal shapes. This can be explained by the fact that the values of the exchange current densities on different crystal planes are quite different, whereas the reversible potential is approximately the same for all planes [10, 11]. This can lead to preferential growth of some crystal planes, because the rate of deposition depends only on the orientation, which leads to the formation of a large-grained rough deposit. However, even at low

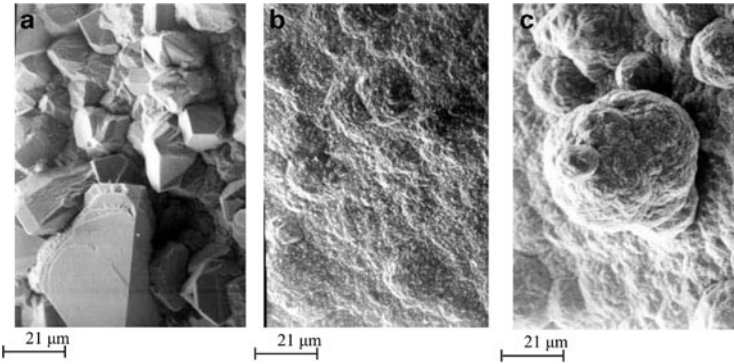


Fig. 1.2 Copper deposits obtained from 0.10 M CuSO_4 in 0.50 M H_2SO_4 . Quantity of electricity, Q : 20 mAh cm^{-2} . (a) Activation-controlled deposition: deposition overpotential, η : 90 mV, initial current density: 3.3 mA cm^{-2} ; (b) electrodeposition under mixed activation–diffusion control: $\eta = 140$ mV, initial current density: 4.2 mA cm^{-2} , and (c) electrodeposition under dominant diffusion control: $\eta = 210$ mV, initial current density 6.5 mA cm^{-2} (Reprinted from [7, 10] with permission from Springer and [12] with permission from Elsevier.)

degrees of diffusion control, the formation of large, well-defined grains is not to be expected, because of irregular growth caused by mass transport limitations. Hence, the current density which corresponds to the very beginning of mixed control (a little larger than this at the end of the Tafel linearity) will be the optimum one for compact metal deposition [12].

All the above facts are illustrated in Fig. 1.2 [12].

1.2.2.2 Cauliflower-Like Forms

It can be seen from Fig. 1.2c that the surface protrusions are globular and cauliflower-like. If the initial electrode surface protrusions are ellipsoidal shape, they can be characterized by the base radius R_0 and the height h as shown in Fig. 1.3a.

The tip radius is then given by

$$r = \frac{R_0^2}{h}. \quad (1.28)$$

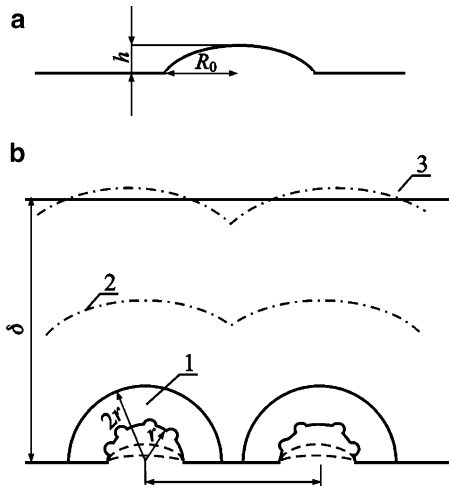


Fig. 1.3 Schematic representation of (a) the initial electrode surface protrusion and (b) the establishment of spherical diffusion layers around independently growing protrusions. (1) $r < (\delta - h)$ and $r < 1/4 l$, spherical diffusion zones are formed; (2) $r < (\delta - h)$ and $r > 1/4 l$, spherical diffusion zones overlap; (3) $r > (\delta - h)$, spherical diffusion zones are not formed (Reprinted from [13] with permission from the Serbian Chemical Society and [7, 10] with permission from Springer.)

The initial electrode surface protrusion is characterized by $h \rightarrow 0$ and $r \rightarrow \infty$ if $R_0 \neq 0$. In this situation, a spherical diffusion layer cannot be formed around the tip of the protrusion if $r < \delta - h$, and linear diffusion control occurs, leading to an increase in the height of the protrusion relative to the flat surface.

The rate of growth of the tip of a protrusion for $r > \delta$ is equal to the rate of motion of the tip relative to the rate of motion of the flat surface. Hence,

$$\frac{dh}{dt} = \frac{V}{nF} (j_{L, \text{tip}} - j_L). \quad (1.29)$$

Substituting $j_{L, \text{tip}}$ from Eq. (1.16) and j_L from Eq. (1.5) in Eq. (1.29) and further rearranging gives

$$\frac{dh}{dt} = \frac{VDC_0}{\delta} h \quad (1.30)$$

or

$$h = h_0 \exp\left(\frac{VDC_0}{\delta^2} t\right). \quad (1.31)$$

When h increases, r decreases, and spherical diffusion control can be operative around the whole surface of protrusion, if it is sufficiently far from the other ones, as illustrated by Fig. 1.3b. In this situation, second-generation protrusions can grow inside the diffusion layer of first-generation protrusions in the same way as first-generation protrusions grow inside the diffusion layer of the macroelectrode and so on.

A cauliflower-like deposit is formed under such conditions, as is shown in Fig. 1.4. It can be seen from Fig. 1.4a that the distance between the cauliflower-like grains is sufficiently large to permit the formation of spherical diffusion zones around each of them. Simultaneously, second-generation protrusions grow in all directions, as shown in Fig. 1.4b, c. This confirms the assumption that the deposition takes place in a spherically symmetric fashion.

To a first approximation, the rate of propagation can be taken to be practically the same in all directions, meaning that the cauliflower-type deposit formed by spherically symmetric growth inside the diffusion layer of the macroelectrode will be hemispherical, as is illustrated in Fig. 1.4a–c.

This type of protrusion is much larger than that formed by linearly symmetric growth inside the diffusion layer of the macroelectrode (Fig. 1.4a–c).

This is because a spherical diffusion layer cannot be formed around closely packed protrusions, their diffusion fields overlap and they grow in the diffusion layer of the macroelectrode.

If spherical diffusion layer can be established around the tip of a protrusion the limiting diffusion current to the tip is given by Eq. (1.19) or by

$$j_{L,\text{tip}} = j_L \frac{h}{r} \quad (1.32)$$

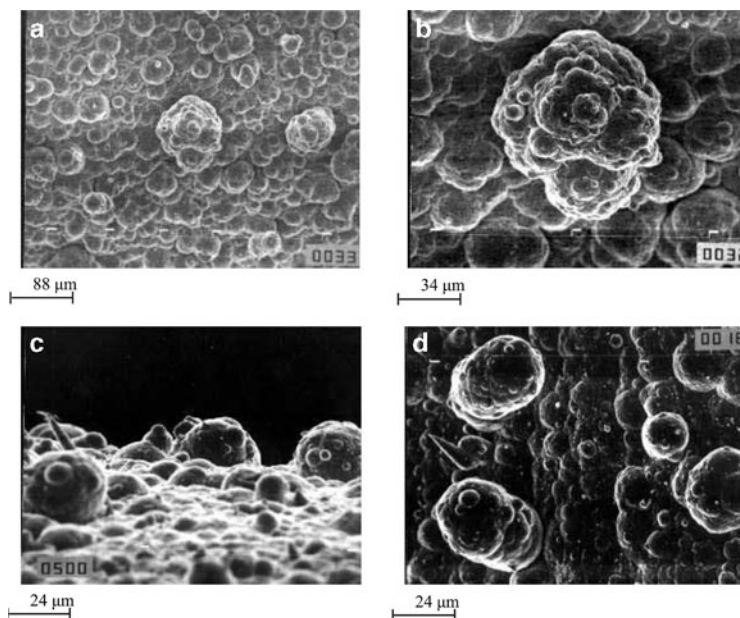


Fig. 1.4 Copper deposits obtained from 0.30 M CuSO_4 in 0.50 M H_2SO_4 by electrodeposition under mixed activation–diffusion control. Deposition overpotential: 220 mV (a) Quantity of electricity: 40 mAh cm^{-2} ; (b) The same as in (a), and (c) and (d) quantity of electricity: 20 mAh cm^{-2} (Reprinted from [7, 10] with permission from Springer and [13] with permission from the Serbian Chemical Society.)

for

$$\frac{h}{r} \gg 1. \quad (1.33)$$

1.2.2.3 Carrot-Like Forms

It can also be seen from Figs. 1.4c, d and 1.5 that the growth of such protrusions produces carrot-like forms, another typical form obtained in copper deposition under mixed activation–diffusion control. This happens under the condition $k \ll 1$, when spherical diffusion

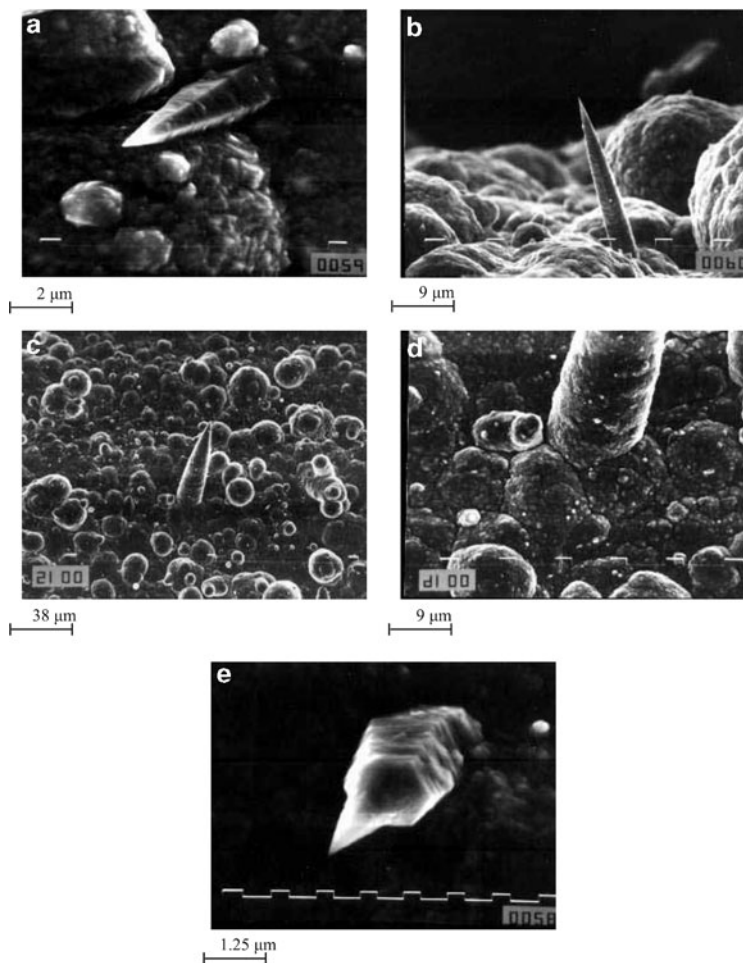


Fig. 1.5 Copper deposits obtained from 0.30 M CuSO_4 in 0.50 M H_2SO_4 by electrodeposition under mixed activation–diffusion control. Deposition overpotential: 220 mV. Quantity of electricity (a) 10 mAh cm^{-2} ; (b) 40 mAh cm^{-2} ; (c) 20 mAh cm^{-2} ; (d) the root of the carrot from (c); and (e) 10 mAh cm^{-2} (Reprinted from [7, 10] with permission from Springer and [14] with permission from the Serbian Chemical Society.)

control takes place only around the tip of the protrusion, as is illustrated in Fig. 1.5. In this case, Eq. (1.27) can be rewritten in the form:

$$j_{\text{tip}} = j_{0,\text{tip}}(f_c - f_a), \quad (1.34)$$

meaning that deposition on the protrusion tip can be under pure activation control at overpotentials lower than the critical one for the initiation of dendritic growth.

This happens if the nuclei have a shape like that in Fig. 1.5. The assumption that the protrusion tip grows under activation control is confirmed by the regular crystallographic shape of the tip [14] just as in the case of grains growing on the macroelectrode under activation control (see Fig. 1.2a).

The maximum growth rate at a given overpotential corresponds to activation-controlled deposition. As a result, the propagation rate at the tip will be many times larger than that in other directions, resulting in protrusions like that in Fig. 1.5b. The final form of the carrot-like protrusion is shown in Fig. 1.5c. It can be concluded from the parabolic shape that such protrusions grow as moving paraboloids in accordance with the Barton–Bockris theory [5], the tip radius remaining constant because of the surface energy effect. It can be concluded from Fig. 1.5d that thickening of such a protrusion is under mixed activation–diffusion control because the deposit is seen to be of the same quality as that on the surrounding macroelectrode surface. It can be seen from Fig. 1.5e that activation control takes place only at the very tip of the protrusion.

1.2.3 The Essence of Dendritic Deposits Formation

Two phenomena seem to distinguish dendritic from carrot-like growth [15–17]:

1. A certain well-defined critical overpotential value appears to exist below which dendrites do not grow.
2. Dendrites exhibit a highly ordered structure and grow and branch in well-defined directions. According to Wranglen [18], a dendrite is a skeleton of a monocrystal and consists of a stalk and branches, thereby resembling a tree.

It is known that dendritic growth occurs selectively at three types of growth sites [16]:

1. Dendritic growth occurs at screw dislocations. Sword-like dendrites with pyramidal tips are formed by this process [3, 16].
2. Many investigations of the crystallographic properties of dendrites have reported the existence of twin structures [19–21]. In the twinning process, a so-called indestructible reentrant groove is formed. Repeated one-dimensional nucleation in the groove is sufficient to provide for growth extending in the direction defined by the bisector of the angle between the twin plants [16].
3. It is a particular feature of a hexagonal close-packed lattice that growth along a high-index axis does not lead to the formation of low index planes. Grooves containing planes are perpetuated and so is the chance for extended growth by the one-dimensional nucleation mechanism [22].

In all the above cases, the adatoms are incorporated into the lattice by repeated one-dimensional nucleation. On the other hand, deposition to the tip of screw dislocations can be theoretically considered as deposition to a point; in the other two cases, the deposition is to a line.

From the electrochemical point of view, a dendrite can be defined as an electrode surface protrusion that grows under activation or mixed control, while deposition to the flat part of the electrode surface is under complete diffusion control [3, 4, 8, 15].

Considering the model of surface irregularities shown in Fig. 1.1, the surface irregularities are buried deep in the diffusion layer, which is characterized by a steady linear diffusion to the flat portion of completely active surface.

If the protrusion does not affect the outer limit of the diffusion layer, i.e., if $\delta \gg h$, the limiting diffusion current density to the tip of the protrusion from Fig. 1.1, $j_{L,\text{tip}}$, is given by

$$j_{L,\text{tip}} = j_L \left(1 + \frac{h}{r} \right). \quad (1.19)$$

Substitution of $j_{L,\text{tip}}$ from Eq. (1.19) into Eq. (1.1) produces for $h/r \gg 1$:

$$j_{\text{tip}} = j_{0,\text{tip}}(f_c - f_a), \quad (1.34)$$

where $j_{0,\text{tip}}$ is the exchange current density at the tip of a protrusion.

Obviously, deposition to the tip of such protrusion inside the diffusion layer is activation-controlled relative to the surrounding electrolyte, but it is under mixed activation–diffusion control relative to the bulk solution.

If deposition to the flat part of electrode is a diffusion-controlled process and assuming a linear concentration distribution inside diffusion layer, the concentration C_{tip} at the tip of a protrusion can be given by modified Eq. (1.17) [3]

$$C_{\text{tip}} = C_0 \frac{h}{\delta}. \quad (1.17a)$$

According to Newman [23] the exchange current density at the tip of a protrusion is given by

$$j_{0,\text{tip}} = j_0 \left(\frac{C_{\text{tip}}}{C_0} \right)^\xi, \quad (1.35)$$

where

$$\xi = \frac{d \log j_0}{d \log C_0} \quad (1.36)$$

and j_0 is the exchange current density for a surface concentration C_0 equal to that in the bulk,

or

$$j_{0,\text{tip}} = j_0 \left(\frac{h}{\delta} \right)^\xi \quad (1.37)$$

because of Eq. (1.17a).

Taking into account Eq. (1.34), the current density to the tip of a protrusion is then given by

$$j_{\text{tip}} = j_0 \left(\frac{h}{\delta} \right)^\xi (f_c - f_a) \quad (1.38)$$

being under mixed control due to the $(h/\delta)^\xi$ term, which takes into account the concentration dependence of $j_{0,\text{tip}}$, expressing in this way a mixed-controlled electrodeposition process.

Outside the diffusion layer $h \geq \delta$, Eq. (1.38) becomes

$$j_{\text{tip}} = j_0 (f_c - f_a), \quad (1.39)$$

indicating pure activation control, as the $(h/\delta)^\xi$ term is absent.

For the dendrite growth, the current density to the tip of a protrusion formed on the flat part of the electrode surface growing inside the diffusion layer should be larger than the corresponding limiting diffusion current density [24]. Hence,

$$j_L < j_{\text{tip}}, \quad (1.40)$$

the protrusion grows as a dendrite.

In accordance with Eq. (1.40), instantaneous dendrite growth is possible at overpotentials larger than some critical value, η_c , which can be derived from Eq. (1.38) as shown in [15, 17]

$$\eta_c = \frac{b_c}{2.3} \ln \frac{j_L}{j_0} \left(\frac{\delta}{h} \right)^\xi, \quad (1.41)$$

and minimum overpotential at which dendritic growth is still possible, η_i is given by

$$\eta_i = \frac{b_c}{2.3} \ln \frac{j_L}{j_0} \quad (1.42)$$

for $f_c \gg f_a$, where h and δ are the protrusion height and the diffusion layer thickness, respectively. For very fast processes, when $j_0/j_L \gg 1$, and if $f_c \approx f_a$ but $f_c > f_a$, Eq. (1.41) becomes

$$\eta_c = \frac{RT}{nF} \frac{j_L}{j_0} \left(\frac{\delta}{h} \right)^\xi \quad (1.43)$$

and Eq. (1.42)

$$\eta_i = \frac{RT}{nF} \frac{j_L}{j_0}, \quad (1.44)$$

meaning that in the case of ohmic-controlled reactions, dendritic growth can be expected at very low overpotentials, or better to say, if $j_0 \rightarrow \infty$, instantaneous dendritic growth is possible at all overpotentials if only mass transfer limitations are taken into consideration.

In fact, dendrite propagation under such conditions is under diffusion and surface energy control, and η_c is then given by [5, 24]

$$\eta_c = \frac{8\sigma V}{nFh} \quad (1.45)$$

where σ is the interfacial energy between metal and solution and V is the molar volume of the metal, and minimum overpotential at which dendritic growth is still possible, η_i is given by

$$\eta_i = \frac{8\sigma V}{nF\delta}. \quad (1.46)$$

Hence, a critical overpotential for initiation dendritic growth is also expected in such cases, being of the order of few millivolts [15, 17, 24].

1.3 Polarization Curves

1.3.1 *The Polarization Curve Equation for Partially Covered Inert Electrode*

A mathematical model can be derived under the assumption that the electrochemical process on the microelectrodes inside the diffusion layer of a partially covered inert macroelectrode is under activation control, despite the overall rate being controlled by the diffusion layer of the macroelectrode [6, 25]. The process on the microelectrodes

decreases the concentration of the electrochemically active ions on the surfaces of the microelectrodes inside the diffusion layer of the macroelectrode, and the zones of decreased concentration around them overlap, giving way to linear mass transfer to an effectively planar surface [26]. Assuming that the surface concentration is the same on the total area of the electrode surface, under steady-state conditions, the current density on the whole electrode surface, j , is given by

$$j = \frac{nFD(C_0 - C_S)}{\delta}, \quad (1.47)$$

where n is the number of transferred electrons, F is the Faraday constant, and D is the diffusion coefficient of the reacting ion. Obviously, the current density from Eq. (1.47) is due to the difference in the bulk, C_0 , and surface concentration, C_S , of the reactive ion. The concentration dependence of the exchange current density [23] is expressed as

$$j_{0,S} = \left(\frac{C_S}{C_0}\right)^\xi j_0, \quad (1.48)$$

where $j_{0,S}$ is the exchange current density for a surface concentration C_S .

The current density on the macroelectrode can also be written as

$$j = S_w j_0 \left(\frac{C_S}{C_0}\right)^\xi (f_c - f_a), \quad (1.49)$$

assuming a reversible activation-controlled electrode process on the hemispherical active microelectrodes on an inert substrate, where S_w is the active surface per square centimeter of the macroelectrode, and j_0 is the exchange current density on the massive active electrode, standardized to the apparent electrode surface.

The current densities given by Eqs. (1.47) and (1.49) are mutually equal and substitution of C_S/C_0 from Eq. (1.47) into Eq. (1.49) gives

$$j = S_w j_0 \left(1 - \frac{j}{j_L}\right)^\xi (f_c - f_a). \quad (1.50)$$

Different forms of polarization curve equation were discussed in detail [25] and this form was chosen for digital simulation. The use of any other form of the polarization curve equation will give some similar results.

1.3.2 Calculated Polarization Curves When Ohmic Potential Drop Is Not Included

The shape of polarization curves can be estimated by digital simulation [6]. It will be performed for example for one-electron transfer process and $\beta = 0.5$ and $\xi = 0.5$. In all cases the apparent current density is standardized to the apparent surface of modified electrode.

Using Eq. (1.50) with $\xi = 0.5$ and $j_0/j_L = 100, 1,$ and $0.01,$ $S_w = 0.05, 0.1, 0.25, 0.5, 0.75,$ and $1,$ and $f_c = 10^{\frac{\eta}{120}}$ and $f_a = 10^{-\frac{\eta}{120}},$ the diagrams presented in Fig. 1.6 are obtained. The current density–overpotential dependence above each set of polarization curves corresponds to $S_w = 1.$ It follows from Fig. 1.6 that for large values of $j_{0,eff}/j_L,$ electrochemical polarization can probably be neglected and that complete ohmic control of the deposition process can be expected, for $j_{0,eff}/j_L \geq 100$ up to a current density about $0.95 j_L$ and for $j_{0,eff}/j_L = 0.5$ for current densities lower than $0.3 j_L.$

As told earlier, the shape of polarization curves does not depend strongly on S_w at large j_0/j_L ratios. At lower ones the important effect arises.

1.3.3 Calculated Polarization Curves with Included Ohmic Potential Drop

The polarization curves for the electrodeposition process which include the ohmic voltage drop can be obtained as follows, assuming $S_w = 1$ in all cases [25, 27]. This will be performed for a one-electron transfer process and $\beta = 0.5,$ meaning $\xi = 0.5$ [6].

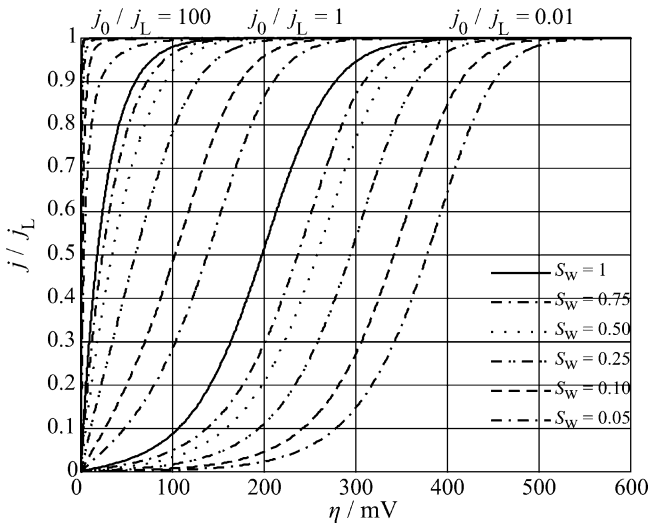


Fig. 1.6 Dependences $j/j_L - \eta$ calculated from Eq. (1.50), using $j_0/j_L = 100, 1,$ and 0.01 , $S_w = 0.05, 0.1, 0.25, 0.5, 0.75,$ and 1 , $f_c = 10^{\frac{\eta}{120}}$, $f_a = 10^{-\frac{\eta}{120}}$, and $\xi = 0.5$ (Reprinted from [6] with permission from Elsevier and [25] with permission from Springer.)

Using Eq. (1.50) with $\xi = 0.5$ and $j_0/j_L = 100, 10, 1,$ and 0.01 , $f_c = 10^{\frac{\eta}{120}}$, $f_a = 10^{-\frac{\eta}{120}}$, and $j_L = 50 \text{ mA cm}^{-2}$, the dependences presented by the dashed line in Figs. 1.7 and 1.8 are obtained. The ohmic potential drop is not included in the calculated polarization curves depicted in Figs. 1.7 and 1.8 by the dashed line. It follows from Figs. 1.7 and 1.8 that for large values of j_0/j_L , electrochemical polarization can probably be neglected but mass transfer limitations are present in all cases, which can also be shown by differentiation of Eq. (1.1).

On the other hand, the measured value of overpotential, η_m , is given by

$$\eta_m = \eta + j \frac{L}{\kappa} \quad (1.51)$$

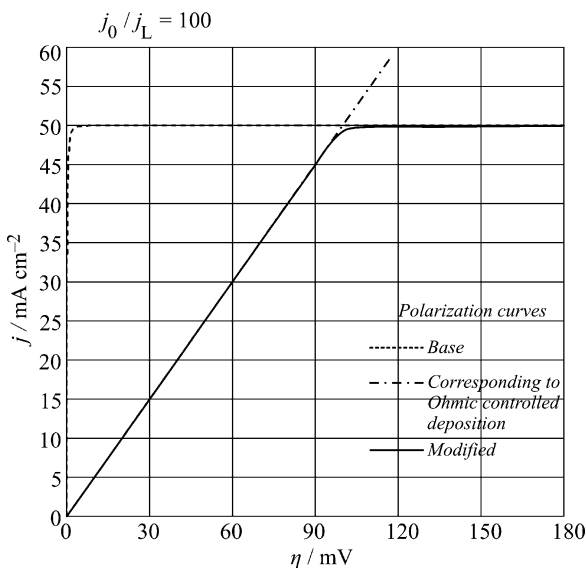


Fig. 1.7 The dependence $j - \eta$ calculated using Eq. (1.50), $j_0/j_L = 100$, $f_c = 10^{1/20}$, $f_a = 10^{-1/20}$, $\xi = 0.5$, $S_w = 1$, and $j_L = 50 \text{ mA cm}^{-2}$, and one modified using Eq. (1.51), $L = 0.2 \text{ cm}$, $\kappa = 0.1 \text{ S cm}^{-1}$ (Reprinted from [27] with permission from Elsevier and [25] with permission from Springer.)

due to the IR error [28], where L is the length of the electrolyte column between the tip of a liquid capillary and the electrode and κ is the specific conductivity of the electrolyte.

For a 1 M solution of a typical fully dissociated electrolyte, the value of κ is around 0.1 S cm^{-1} , L can be taken as 0.2 cm and $j_L = 50 \text{ mA cm}^{-2}$. Using these given values, as well as $\kappa = 0.033 \text{ S cm}^{-1}$, Eq. (1.51), and the diagrams presented in Figs. 1.7 and 1.8 by the dashed line, polarization curves including the ohmic potential drop can be obtained, as shown in Figs. 1.7 and 1.8 by the solid line.

In the case under consideration, complete ohmic control of the deposition process can be expected for $j_0/j_L \geq 100$ up to a current density about $0.95j_L$ (Fig. 1.7). It is obvious from Figs. 1.7 and 1.8 that, regardless of the shape of the polarization curve which depends

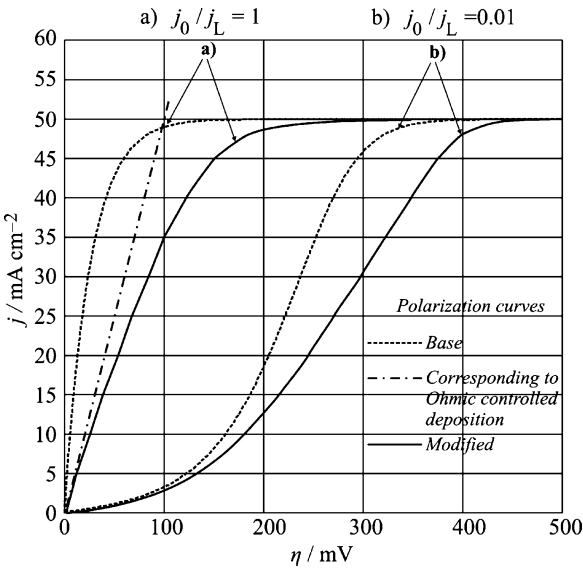


Fig. 1.8 The dependences $j - \eta$ calculated using Eq. (1.50), $j_0/j_L = 1$ and 0.01 , $f_c = 10^{n/120}$, $f_a = 10^{-n/120}$, $\xi = 0.5$, $S_w = 1$, and $j_L = 50 \text{ mA cm}^{-2}$, and ones modified using Eq. (1.51), $L = 0.2 \text{ cm}$, $\kappa = 0.1 \text{ S cm}^{-1}$ (Reprinted from [27] with permission from Elsevier and [25] with permission from Springer.)

on the j_0/j_L ratio and κ , a limiting diffusion current density plateau is present in all cases.

It can be noticed that before the increase of the current density, over the value of the limiting diffusion one, the first part of the polarization curve for silver deposition from nitrate solution [6] has practically the same shape as that from Fig. 1.7 and that those from Fig. 1.8 are very similar to the ones for Cd and Cu deposition [29]. The value of j_0 for Ag deposition is very large [30]. In the cases of both Cd [31] and Cu [32] deposition, j_0 is considerably lower than in the case of Ag deposition.

The increase in the current density over the limiting diffusion current in the absence of some other electrochemical process indicates a decrease of the mass transport limitations, due to initiation of growth of dendrites and further dendritic growth.

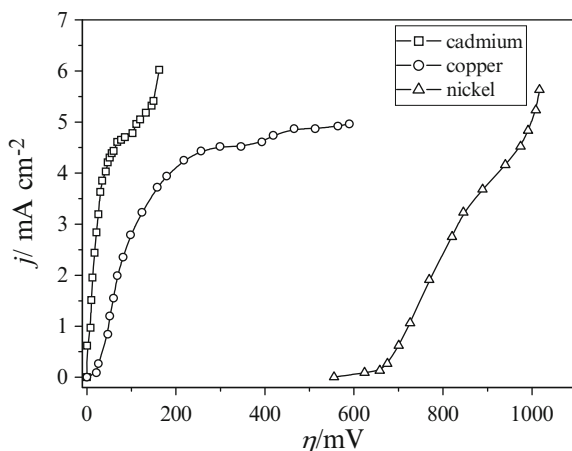


Fig. 1.9 Polarization curve for cadmium (*open square*), copper (*open circle*) and nickel (*open triangle*) depositions (Reprinted from [33] with permission from the Serbian Chemical Society.)

Table 1.1 The exchange current density and j_L/j_0 ratios for Cd, Cu, and Ni deposition processes

Metal	j_0 (A cm^{-2})	j_L/j_0
Cadmium	1.5×10^{-3}	3.0
Copper	3.2×10^{-4}	14.4
Nickel	1.6×10^{-9}	2.9×10^6

Reprinted from [33] with permission from Serbian Chemical Society and [15] with permission from Springer

1.3.4 Polarization Curves Measured for Different j_0/j_L Ratios

The polarization curves for nickel, copper, and cadmium deposition are shown in Fig. 1.9, while corresponding Tafel plots and the results of linear polarization experiments are given in [33]. The limiting diffusion currents in all cases are practically the same, but the exchange current densities (given in Table 1.1) are very different.

The shape of polarization curves is qualitatively in accordance with polarization curves presented in Figs. 1.6–1.8 due to the different j_0/j_L ratios.

1.4 Dendritic Growth Initiation Inside Diffusion Layer of the Macroelectrode

1.4.1 Ohmic-Controlled Deposition

The initiation of dendritic growth is followed by an increase of the deposition current density, and the overall current density will be larger than the limiting diffusion current on a flat active electrode. Based on the above discussion, the polarization curve equation in the ohmic-controlled electrodeposition of metals can be determined now by [27]

$$j = \frac{\kappa\eta}{L} \quad \text{for} \quad 0 \leq \eta < j_L \frac{L}{\kappa}, \quad (1.52a)$$

$$j = j_L \quad \text{for} \quad j_L \frac{L}{\kappa} \leq \eta < \eta_c + j_L \frac{L}{\kappa}, \quad (1.52b)$$

$$j = j_L \theta + (1 - \theta)j_0 \frac{(f_c - f_a)}{N} \sum_{i=1}^{i=N} \left(\frac{h_i}{\delta} \right)^\xi, \quad \text{for} \quad \eta_c \leq \eta, \quad (1.52c)$$

where $N = N(t)$ is the number of dendrites and $\theta = \theta(t) \leq 1$, where θ is the flat part of the electrode surface.

Equation (1.52a) describes the linear part of the polarization curves for tin [34], silver [6] and lead [35] deposition, and Eq. (1.52b) foresees the inflection point in the cases when η_c is low and the resistance of the electrolyte is large. Finally, Eq. (1.52c) describes the part of the polarization curve after initiation of dendrite growth.

The exchange current density of the silver reaction in nitrate electrolytes is sufficiently large to permit ohmic-controlled deposition, as well as dendritic growth at low overpotentials [30].

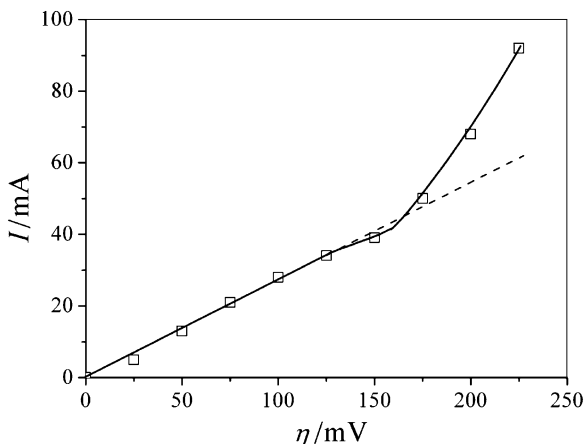


Fig. 1.10 The polarization curve for silver electrodeposition from nitrate solution on a graphite electrode (Reprinted from [27] with permission from Elsevier and [36] with permission from Springer.)

After a linear increase of the deposition current density with increasing overpotential, an exponential increase after the inflection point appears, meaning the elimination of mass transfer limitations due to the initiation of dendritic growth. Thus, instead of a limiting diffusion current density plateau, a curve inflection point or a short inclined plateau can be expected on the polarization curve in ohmic-controlled electrodeposition of metals, as observed.

The polarization curve for silver electrodeposition from nitrate solution, 0.50 M AgNO_3 in 0.20 M HNO_3 , onto a graphite electrode is shown in Fig. 1.10. The overpotential was increased from the initial to the final value and held for 30 s before measurement in all cases during the polarization measurements. The polarization curve in Fig. 1.10 means that mass transfer limitations were decreased or even eliminated. The SEM photomicrographs of the deposit corresponding to the points from Fig. 1.10 are shown in Fig. 1.11.

It can be seen from Figs. 1.10 and 1.11a that at an overpotential of 100 mV, only grains [27] can be seen, which means that the deposition was not under diffusion control. It follows from Figs. 1.10 and 1.11b that deposition at an overpotential of 125 mV is still out of

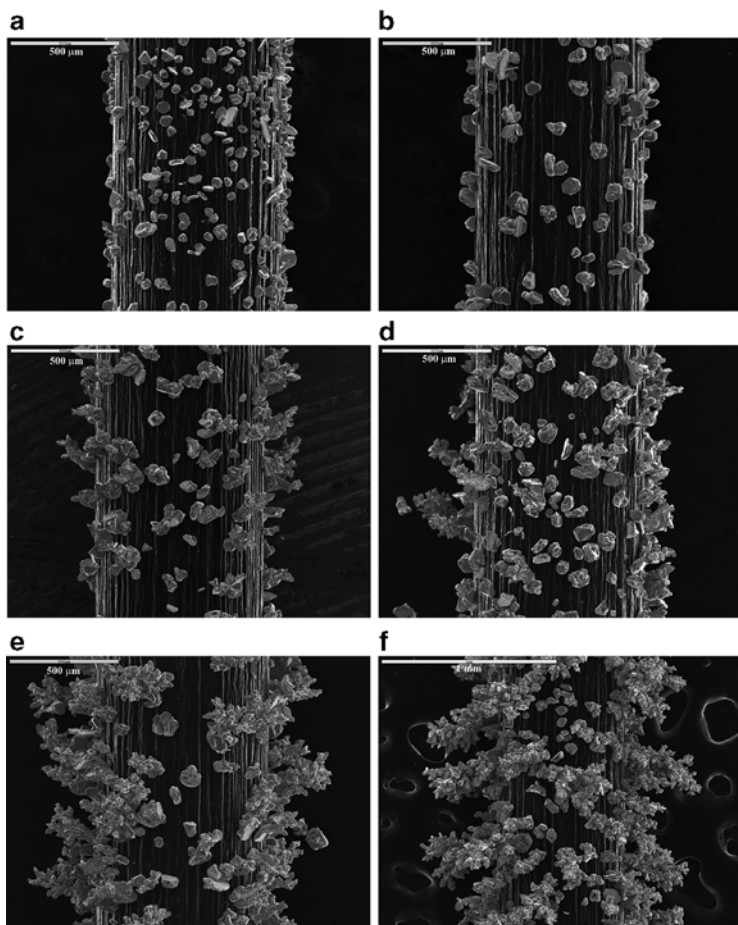


Fig. 1.11 The SEM photomicrographs of the silver deposit obtained on a graphite electrode obtained after the recording of the current at different overpotentials in polarization measurements (a) 100 mV; (b) 125 mV; (c) 150 mV; (d) 175 mV; (e) 200 mV; and (f) 225 mV (Reprinted from [27] with permission from Elsevier and [36] with permission from Springer.)

diffusion control. At 150 mV, the current density is somewhat lower than that which could be expected from the linear dependence of current on overpotential. This indicates the initiation of diffusion control of the deposition process, but also the initiation of dendrite growth, which compensates the mass transfer limitations, as can be seen from Figs. 1.10 and 1.11c. The point corresponding to an overpotential of 150 mV can be considered as the inflection point of the polarization curve in Fig. 1.10.

At overpotentials larger than 175 mV, the current density is considerably larger than the one expected from the linear dependence of current on overpotential. The formation of dendritic deposits (Fig. 1.11d–f) confirms that the deposition was dominantly under activation control. Thus, the elimination of mass transport limitations in the ohmic-controlled electrodeposition of metals is due to the initiation of dendritic growth at overpotentials close to that at which complete diffusion control of the process on the flat part of the electrode surface occurs.

It is necessary to note that the silver deposits shown in Fig. 1.11d–f are not similar to ideal silver dendrites [18], but they behave as dendritic ones in regard to their electrochemical properties. Hence, they can be considered as degenerate dendritic deposits.

Occasionally, the needle-like dendrites can also be formed.

1.4.2 Ohmic-Diffusion and Activation–Diffusion Controlled Deposition

In these cases the dendritic growth starts at overpotentials larger than the one which corresponds to the beginning of the limiting diffusion current density plateau [15, 17].

There is an induction period before the initiation of dendritic growth [5]. During this induction period, dendrite precursors are formed and become sufficiently high to satisfy Eq. (1.41) at a given overpotential, as illustrated in Figs. 1.12 and 1.13. The cross-like grains seen in Fig. 1.12a, b further develop into dendrite precursors (Fig. 1.12a, c).

The propagation of this structure by branching (Fig. 1.12d) produces dendrites as shown in Fig. 1.12e.

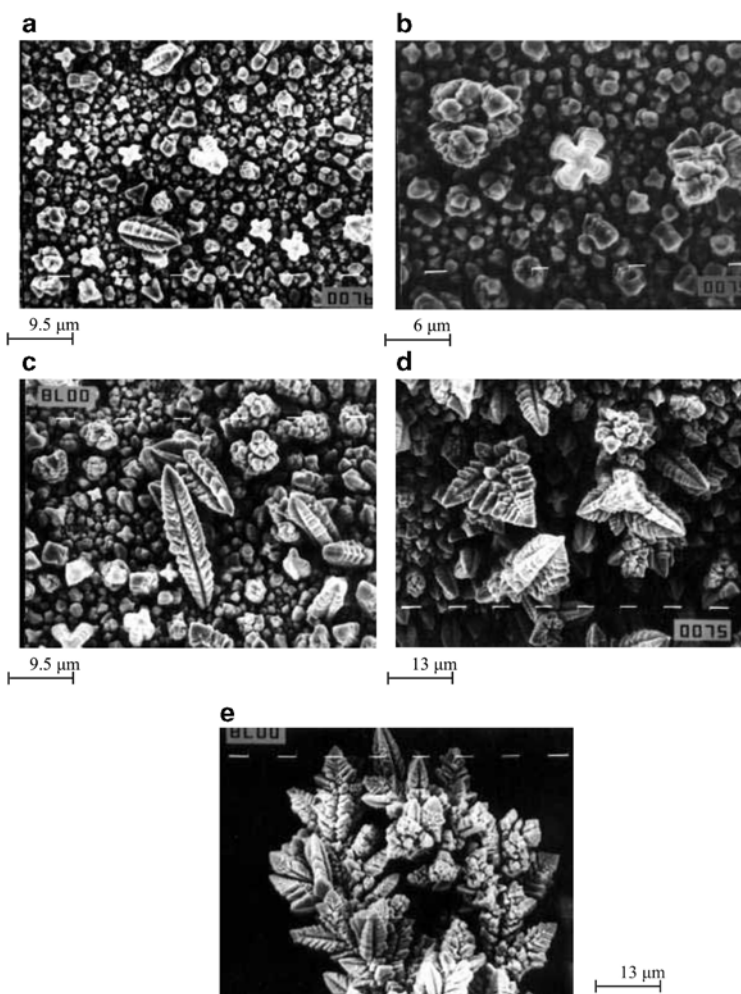


Fig. 1.12 SEM micrographs of copper deposits obtained by deposition from 0.30 M CuSO_4 in 0.50 M H_2SO_4 onto a copper wire electrode. Deposition overpotential: 550 mV. Quantity of electricity: (a) 2 mAh cm^{-2} ; (b) 2 mAh cm^{-2} ; (c) 5 mAh cm^{-2} ; (d) 10 mAh cm^{-2} , and (e) 10 mAh cm^{-2} (Reprinted from [37] with permission from the Serbian Chemical Society and [15, 17] with permission from Springer.)

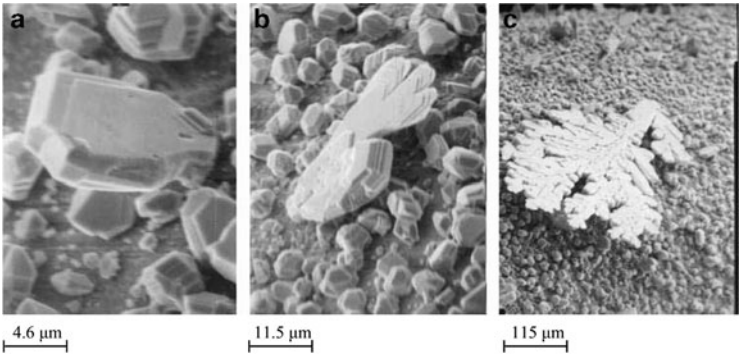


Fig. 1.13 The cadmium deposits obtained by deposition from 0.10 M CdSO₄ in 0.50 M H₂SO₄ onto a cadmium electrode. Deposition overpotential: 50 mV. Deposition times (a) 2 min; (b) 2 min, and (c) 10 min (Reprinted from [38] with permission from Elsevier and [39] with permission from Springer.)

On the other hand, lighter-like precursors from Fig. 1.13a develop in 2D dendrites, as shown in Fig. 1.13c.

The initiation of dendritic growth is followed by a change in the slope of the current density–time curves [15–17], indicating a change in the growth mechanism of the deposit.

The slopes of these dependences are similar to one another and independent of the deposition overpotential during the nondendritic amplification of the surface-coarsening according to Eq. (1.31).

The change of the slope of the current–time dependences due to the dendritic growth initiation will be treated here in somewhat simplified way.

The limiting diffusion current density to the elevated points of a surface protrusion, $j_{L,e}$, is given by

$$j_{L,e} = \frac{nFDC_0}{\delta - h} \quad (1.53)$$

and

$$j_L = \frac{nFDC_0}{\delta} \quad (1.5)$$

to the flat part of the electrode.

The limiting diffusion current density will then be given by

$$j = \theta \frac{nFDC_0}{\delta} + \frac{1 - \theta}{N} \sum_{i=1}^{i=N} \frac{nFDC_0}{\delta - h_i}, \quad (1.54)$$

where θ is the flat part of electrode surface, N is the number of elevated points on the electrode surface, and h_i changes with time according to Eq. (1.55):

$$h_i = h_{0,i} \exp\left(\frac{VDC_0}{\delta^2} t\right), \quad (1.55)$$

which is somewhat modified Eq. (1.31).

It is obvious that dj_L/dt does not depend on overpotential.

After initiation of dendritic growth, the slopes become dependent on the overpotential. A dendrite is a surface protrusion growing under mixed or activation control, while deposition to the flat part of the electrode surface is under complete diffusion control. The overpotential η and current density j_{tip} on the tip of a dendrite are related by

$$j_{\text{tip}} = j_0 \frac{h}{\delta} f_c \quad (1.56)$$

for $f_c \gg f_a$, and Eq. (1.52c) can be rewritten in the form

$$j = j_L \theta + (1 - \theta) j_0 \frac{f_c}{N} \sum_{i=1}^{i=N} \frac{h_i}{\delta}, \quad (1.57)$$

and $\frac{dj}{dt}$ in this case depends on overpotential.

Hence, the maximum overpotential at which the slope of the apparent current density–time dependence remains constant and equal to that in nondendritic amplification of the surface roughness corresponds to η_i . The minimum overpotential at which this slope cannot be recorded corresponds to η_c .

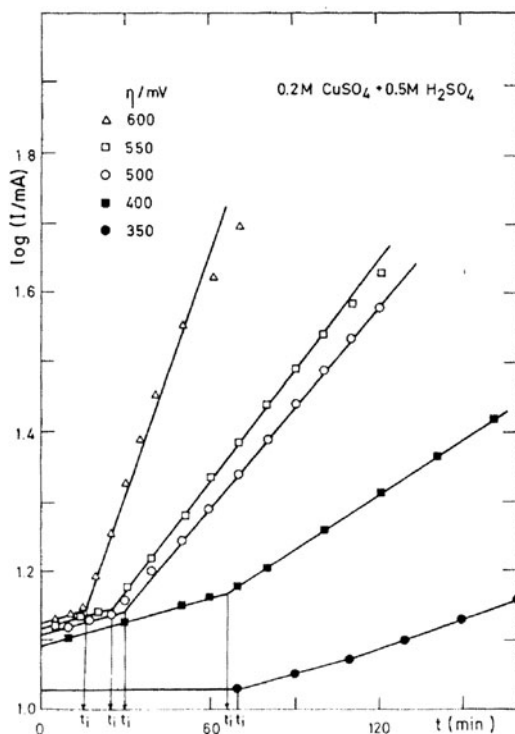


Fig. 1.14 $\log I$ as a function of time for copper deposition (Reprinted from [15, 24, 40] with permission from Springer.)

In this way η_i and η_c can be estimated. It is known that the j - t dependences are different from case to case owing to different mechanisms of dendritic growth initiation and dendritic growth [15]. As a result of this, the analytical approach to the determination of η_i and η_c must be specific for each system under consideration; the procedure for one particular case is as follows.

Typical $\log(\text{current})$ - t dependences obtained for copper deposition from 0.20 M CuSO₄ in 0.50 M H₂SO₄ at overpotentials belonging to the limiting diffusion current plateau are shown in Fig. 1.14. According to the above discussion, it is clear that the

intersection points of the two linear dependencies determines the induction time of dendritic growth initiation [24].

The induction times for dendritic growth initiation extracted from the graphs in Fig. 1.14 can be presented as a function of overpotential, and the critical overpotential for instantaneous dendritic growth can be obtained by extrapolation to zero induction time.

The critical overpotential of dendritic growth initiation can be determined by plotting the logarithm of the slopes of the straight lines from Fig. 1.14 as a function of overpotential, and the intersection point of the two straight lines determines η_i . A similar procedure was followed for the deposition of cadmium from 0.10 M CdSO₄ in 0.50 M H₂SO₄.

The cross sections of the copper and cadmium deposits obtained at $\eta < \eta_i$, $\eta_i < \eta < \eta_c$, and $\eta > \eta_c$ are shown in Figs. 1.15a–c and 1.16a–c, respectively. It can be seen that there is no dendrite formation when $\eta < \eta_i$, both compact and dendritic deposits are formed when $\eta_i < \eta < \eta_c$ and only dendritic metal is deposited when $\eta > \eta_c$. This is in perfect agreement with findings of Calusaru [41] for the morphology of deposits of the same metals deposited at overpotentials corresponding to full diffusion control.

The η_i and η_c of 260 mV and 660 mV for copper deposition (lower j_0 value) and 27 mV and 110 mV for cadmium deposition (larger j_0 value) are successfully determined using the above given procedure, being in perfect agreement with experimental findings as can be seen from Figs. 1.15 and 1.16 [24, 29, 40].

The shapes of the polarization curves presented in Figs. 1.15 and 1.16 are in accordance with values of the exchange current density to the limiting diffusion current density ratios.

It is known [40] that, apart from decreasing the concentration of the depositing ion, the formation of a dendritic deposit can also be enhanced by increasing the concentration of the supporting electrolyte, increasing the viscosity of the solution, decreasing the temperature, and decreasing the velocity of motion of the solution. Practically, all the above facts can be explained by Eqs. (1.42) and (1.44), assuming that a decrease in η_i means enhanced dendrite formation because of the lower electrical work required to produce the dendrites. The possibility of obtaining dendrites of Pb [42] and Sn [43] from aqueous solutions at lower overpotentials than

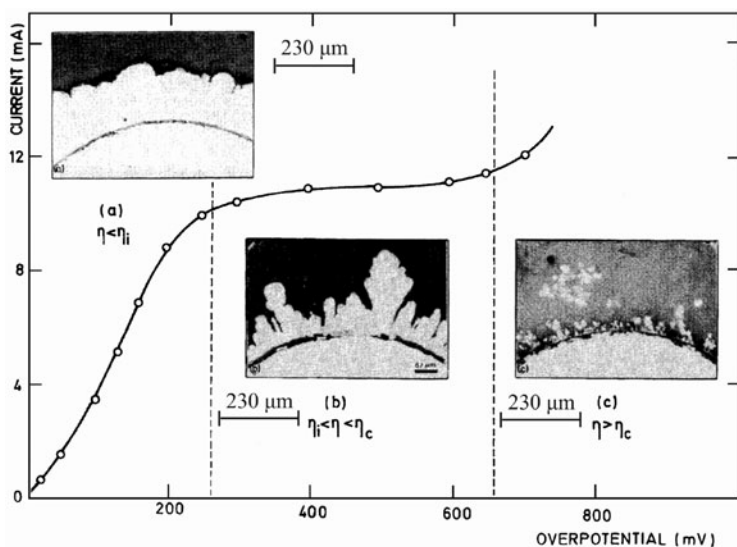


Fig. 1.15 Polarization curve for the potentiostatic deposition of copper from 0.20 M CuSO_4 in 0.50 M H_2SO_4 and the cross sections of copper deposits obtained on copper wire electrodes previously plated with nickel (a) overpotential: 200 mV, deposition time: 6 h; (b) overpotential: 300 mV, deposition time: 5 h, and (c) overpotential: 700 mV, deposition time: 2 min (Reprinted from [24, 29, 40] with permission from Springer and copied by permission from the “Electrochemistry Encyclopedia” (<http://electrochem.cwru.edu/ed/encycl/>) on 04/25/2007. The original material is subject to periodical changes and updates.)

required for the formation of dendrites of Ag from aqueous solutions can also be explained by Eq. (1.46) owing to the much lower melting points of these metals, i.e., their lower surface energy at room temperature. Dendrites of silver can be obtained from molten salts at overpotentials of a few millivolts [5], as in the case of Pb and Sn deposition from aqueous solutions [42, 43], because the difference between the melting point of silver and the working temperature for deposition from molten salts is not very different from the difference between the melting point of lead or tin and room temperature. On the other hand, dendrites grow from screw

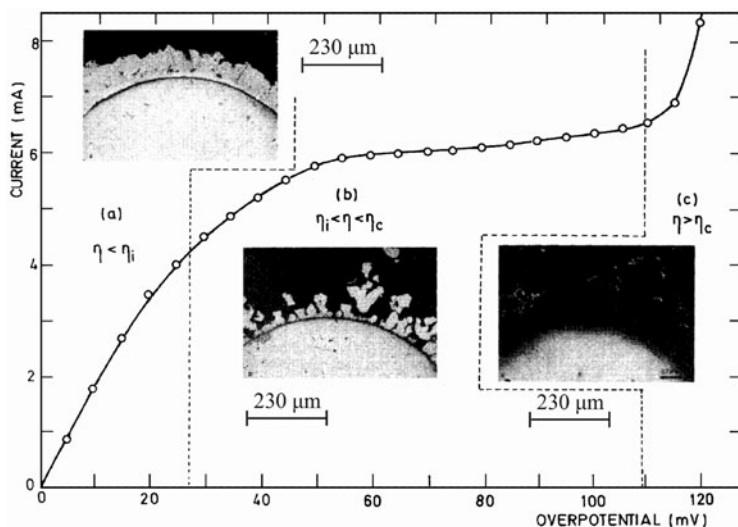


Fig. 1.16 Polarization curve for the potentiostatic deposition of cadmium from 0.10 M CdSO_4 in 0.50 M H_2SO_4 and the cross sections of cadmium deposits obtained on copper wire electrode (a) overpotential: 20 mV, deposition time: 8 h; (b) overpotential: 40 mV, deposition time: 2 h, and (c) overpotential: 120 mV, deposition time: 9 min (Reprinted from [24, 29, 40] with permission from Springer.)

dislocation and nuclei of higher indices or twinned ones only [15–17]. The probability of formation of such nuclei increases with increasing overpotential [44], and η_i can also be defined as the overpotential at which they are formed. Regardless of this, Eqs. (1.42), (1.44), and (1.46) illustrate well the effect of different parameters on the initiation of dendritic growth.

It is obvious that the electrochemical conditions, as well as the crystallographic ones, under which dendritic deposits are formed can be precisely determined. One problem that still seems to remain unsolved is the question what causes the dendrite precursors to appear at regularly spaced locations along the dendrite stem. Further investigations in this direction are necessary.

1.5 Inhibition of Dendritic Growth by Vigorous Hydrogen Codeposition (Formation of the Honeycomb-Like Structures)

Honeycomb-like structures are formed by electrochemical deposition processes at high current densities and overpotentials, where parallel to copper electrodeposition hydrogen evolution reaction occurs. Hydrogen evolution responsible for the formation of this type of structure is vigorous enough to cause such stirring of the solution leading to the change of the hydrodynamic conditions in the near-electrode layer [45].

Figure 1.17 shows the polarization curve for electrodeposition of copper from 0.15 M CuSO_4 in 0.50 M H_2SO_4 . The plateau of the limiting diffusion current density corresponds to the range of overpotentials between 350 and 750 mV. Hydrogen evolution, as the second reaction, commences at some overpotential belonging to the plateau of the limiting diffusion current density, and increasing overpotential intensifies hydrogen evolution reaction. For this copper solution, hydrogen evolution commences at an overpotential of 680 mV [45]. At some overpotential outside the plateau of the

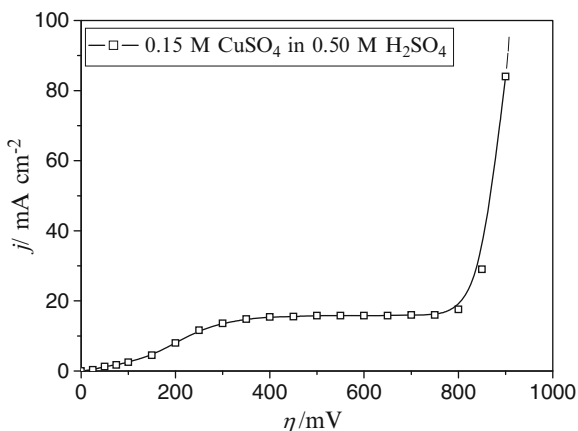


Fig. 1.17 Polarization curve for the cathodic process of copper deposition from 0.15 M CuSO_4 in 0.50 M H_2SO_4 . Temperature: $18.0 \pm 1.0^\circ\text{C}$ (Reprinted from [45] with permission from Elsevier and [46] with permission from Springer.)

Table 1.2 The average current efficiency of hydrogen evolution, $\eta_{l,av}(H_2)$ (%), obtained at overpotentials of 550, 700, 800, and 1,000 mV

Overpotential, η (mV)	550	700	800	1,000
The average current efficiency of hydrogen evolution, $\eta_{l,av}(H_2)$ (%)	0	1.97	10.8	30.0

Reprinted from [45] with permission from Elsevier and [46] with permission from Springer

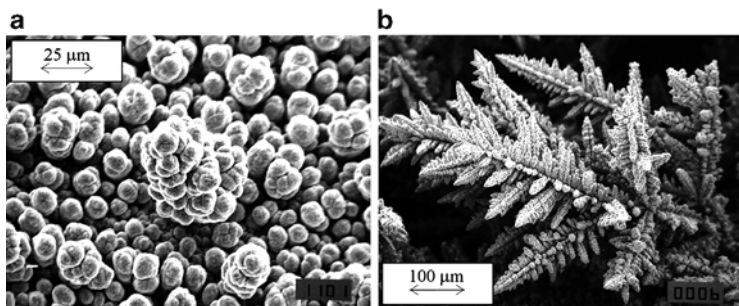


Fig. 1.18 Copper deposits electrodeposited from 0.15 M $CuSO_4$ in 0.50 M H_2SO_4 at overpotentials of (a) 550 mV and (b) 700 mV. The quantity of electricity: 10 mAh cm^{-2} (Reprinted from [45, 47] with permission from Elsevier and [46] with permission from Springer.)

limiting diffusion current density, hydrogen evolution becomes vigorous enough leading to change hydrodynamic conditions in the near-electrode layer [45]. The quantity of evolved hydrogen was quantified by the determination of the average current efficiency for hydrogen evolution reaction, $\eta_{l,av}(H_2)$, and the values obtained at overpotentials belonging to the plateau of the limiting diffusion current density (550 and 700 mV), as well as those obtained outside this plateau (800 and 1,000 mV), are given in Table 1.2.

The typical morphologies of copper deposits obtained at overpotentials belonging to the plateau of the limiting diffusion current density are shown in Fig. 1.18. Cauliflower-like agglomerates of copper grains were formed at an overpotential of 550 mV, where there was no hydrogen evolution (Fig. 1.18a). Very branchy copper dendrites were formed at an overpotential of 700 mV, where hydrogen evolution was very small, and corresponded to the average current efficiency of hydrogen evolution of about 2.0% (Fig. 1.18b) [45].

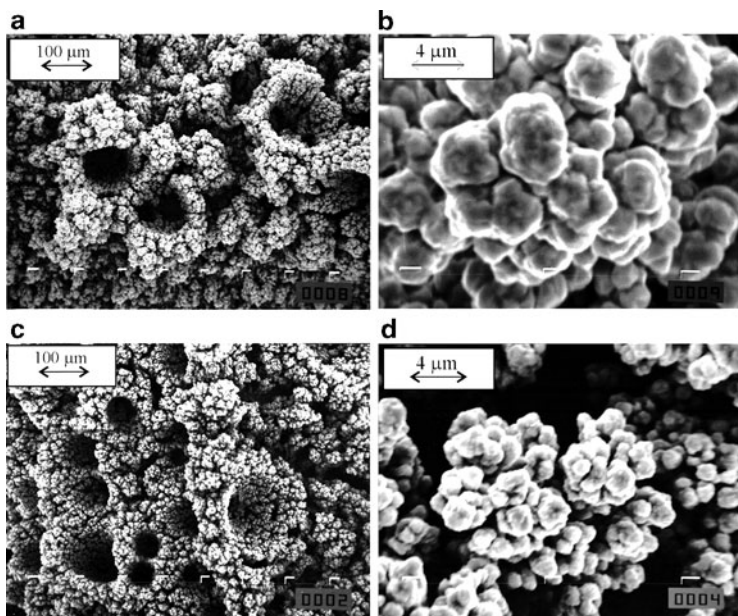


Fig. 1.19 Copper deposits electrodeposited from 0.15 M CuSO_4 in 0.50 M H_2SO_4 at overpotentials of (a) and (b) 800 mV and (c) and (d) 1,000 mV. The quantity of electricity: 10 mAh cm^{-2} (Reprinted from [45, 47] with permission from Elsevier and [46] with permission from Springer.)

Morphologies of copper deposits obtained at overpotentials of 800 and 1,000 mV which were about 50 and 250 mV outside the plateau of the limiting diffusion current density are shown in Fig. 1.19. In both cases holes formed by attached hydrogen bubbles (Fig. 1.19a, c) surrounded by agglomerates of copper grains (Fig. 1.19b, d) were obtained. It is necessary to note that the number of holes formed at an overpotential of 1,000 mV (Fig. 1.19c) was larger than the number of holes formed at an overpotential of 800 mV (Fig. 1.19a). It is understandably due to more vigorous hydrogen evolution at 1,000 mV ($\eta_{\text{L,av}}(\text{H}_2) = 30.0\%$) than at 800 mV ($\eta_{\text{L,av}}(\text{H}_2) = 10.8\%$) [45]. These copper deposits are the typical honeycomb-like structures, and the concept of “effective overpotential” was proposed to explain their formation.

It is known that the hydrogen evolution effects onto the hydrodynamic conditions inside the electrochemical cell [48–50]. The increase in hydrogen evolution rate leads to the decrease of the diffusion layer thickness and hence to the increase of limiting diffusion current density of electrode processes. It was shown [48] that if the rate of gas evolution at the electrode is larger than $100 \text{ cm}^3/\text{cm}^2 \text{ min}$ ($> 5 \text{ A}/\text{cm}^2$), the diffusion layer becomes only a few micrometers thick. It is also shown [47] that a coverage of an electrode surface with gas bubbles can be about 30%. If the thickness of the diffusion layer in conditions of natural convection is $\sim 5 \times 10^{-2} \text{ cm}$ and in strongly stirred electrolyte $\sim 5 \times 10^{-3} \text{ cm}$ [51], it is clear that gas evolution is the most effective way of the decrease of mass transport limitations for electrochemical processes in mixed activation–diffusion control.

For electrochemical process in mixed activation–diffusion control, the overpotential η and the current density j are related by Eq. (1.58) [45]:

$$\eta = \frac{b_c}{2.3} \ln \frac{j}{j_0} + \frac{b_c}{2.3} \ln \frac{1}{1 - \frac{j}{j_L}}. \quad (1.58)$$

The first term in Eq. (1.58) corresponds to the activation part of deposition overpotential and the second one is due to the mass transfer limitations. If one and the same process occurs under two different hydrodynamic conditions, characterized by two different values of the limiting diffusion current densities $j_{L,1}$ and $j_{L,2}$, Eq. (1.58) can be rewritten in the forms

$$\eta_1 = \frac{b_c}{2.3} \ln \frac{j_1}{j_0} + \frac{b_c}{2.3} \ln \frac{1}{1 - \frac{j_1}{j_{L,1}}} \quad (1.59)$$

and

$$\eta_2 = \frac{b_c}{2.3} \ln \frac{j_2}{j_0} + \frac{b_c}{2.3} \ln \frac{1}{1 - \frac{j_2}{j_{L,2}}}, \quad (1.60)$$

where η_1 and η_2 and j_1 and j_2 are the corresponding values of overpotentials and current densities. The same degree of diffusion control is obtained if

$$\frac{j_1}{j_{L,1}} = \frac{j_2}{j_{L,2}} \quad (1.61)$$

or

$$j_2 = j_1 \frac{j_{L,2}}{j_{L,1}} \quad (1.62)$$

and substitution of j_2 from Eq. (1.62) in Eq. (1.61) and further rearranging give

$$\eta_2 = \frac{b_c}{2.3} \ln \frac{j_1}{j_0} + \frac{b_c}{2.3} \ln \frac{1}{1 - \frac{j_1}{j_{L,1}}} + \frac{b_c}{2.3} \ln \frac{j_{L,2}}{j_{L,1}} \quad (1.63)$$

and if Eq. (1.59) is taken into account

$$\eta_2 = \eta_1 + \frac{b_c}{2.3} \ln \frac{j_{L,2}}{j_{L,1}}. \quad (1.64)$$

Hence, if

$$j_{L,2} > j_{L,1} \quad (1.65)$$

to obtain the same degree of diffusion control in two hydrodynamic conditions, Eq. (1.64) must be satisfied, meaning that

$$\eta_2 > \eta_1. \quad (1.66)$$

In the absence of strong hydrogen evolution, the diffusion layer is due to the natural convection and does not depend on the overpotential of electrodeposition. The vigorous hydrogen evolution changes the

hydrodynamic conditions and decreases the degree of diffusion control. Hence, Eq. (1.64) should be rewritten in the form

$$\eta_1 = \eta_2 - \frac{b_c}{2.3} \ln \frac{j_{L,2}}{j_{L,1}}, \quad (1.67)$$

where η_1 becomes the effective overpotential, $\eta_1 = \eta_{\text{eff}}$, related to conditions of natural convection at which there is the same degree of diffusion control as at overpotential η_2 with the hydrogen codeposition. Hence, the dendritic growth can be delayed or completely avoided, as can be seen from Fig. 1.19b, d, meaning that there is a really lower degree of diffusion control at overpotentials of 800 and 1,000 mV with the hydrogen codeposition than at an overpotential of 700 mV where the hydrogen codeposition is very small.

Anyway, the concept of “effective overpotential” can be summarized as follows: when hydrogen evolution is vigorous enough to change hydrodynamic conditions in the near-electrode layer, then electrodeposition process occurs at some overpotential which is effectively lower than the specified one. This overpotential is denoted by “effective overpotential” of electrodeposition process. From morphological point of view, it means that morphologies of metal deposits become similar to those obtained at some lower overpotentials where there is no hydrogen evolution or it is very small. More about the formation of the honeycomb-like structure and the concept of “effective overpotential” can be found in [46, 52–61].

The dendritic growth in this system at larger overpotentials is possible by the application of the appropriate pulsating overpotential (PO) regime. For example, the well-developed dendrites were formed with an overpotential amplitude of 1,000 mV, a deposition pulse, t_c , of 10 ms, and pause, t_p , of 100 ms (the pause to pulse ratio, p , where $p = t_p/t_c = 10$), as shown in Fig. 1.20. Dendrites are formed during the overpotential pulses with the average current density of hydrogen evolution in pulsating conditions which was not vigorous enough to cause the change of hydrodynamic conditions in the near-electrode layer [62, 63].

In the systems characterized by the strong hydrogen evolution which cause the change of hydrodynamic conditions in the near-electrode layer, the formation of dendrites mainly occurs in sheltered parts of the surface area, such as the bottom of holes (Fig. 1.21) [64].

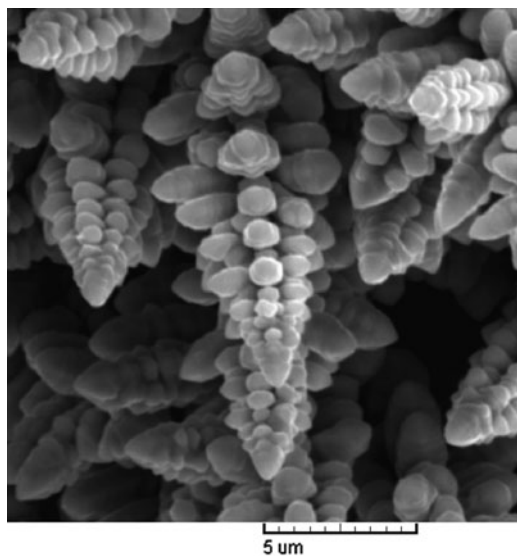


Fig. 1.20 The copper dendrites formed by the pulsating overpotential (PO) regime: deposition pulse of 10 ms, pause duration of 100 ms; deposition time: 18 min; the amplitude overpotential used was 1,000 mV (Reprinted from [62] with permission from Elsevier and [63] from permission from Springer.)

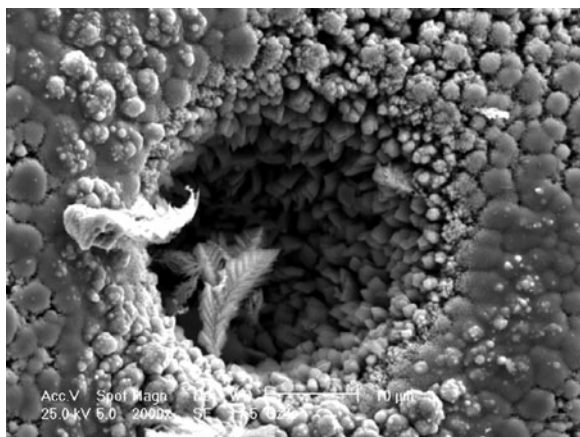


Fig. 1.21 Cobalt powder particle obtained by electrodeposition from a solution containing 1 M $(\text{NH}_4)_2\text{SO}_4$, 0.7 M NH_4OH , and 0.1 M CoSO_4 at a constant current density of 0.5 A cm^{-2} (Reprinted from [64] with permission from Springer.)

1.6 Granular Electrodeposits Formation

Metal electrodeposition on inert electrodes begins with the formation of separate growth centers until a continuous or disperse deposit is produced. Once a nucleus of the depositing metal has been formed, the current flowing causes a local deformation of the electric field in the vicinity of the growing center. As a result, an ohmic potential drop occurs along the nucleus-anode direction. Considering the high dependence of the nucleation rate on the overpotential, new nuclei would be expected to form only outside the spatial region around the initial nucleus. In that region the potential difference between the cathode and the electrolyte surpasses some critical value η_{cr} . Using simple mathematics, one obtains for the radius of the screening zone, r_{sz} , in an ohmic-controlled deposition:

$$r_{sz} = f \frac{U_{\Omega}}{U_{\Omega} - \eta_{cr}} r_N, \quad (1.68)$$

where η_{cr} is the critical overpotential for nucleation to occur, U_{Ω} is the ohmic drop between the anode and cathode, f is a numerical factor, and r_N is the radius of the nucleus. The radius of the screening zone depends on the value of both U_{Ω} and η_{cr} . At a constant η_{cr} , an increase in U_{Ω} leads to a decrease in the radius of the screening zone; the same is true if η_{cr} decreases at constant U_{Ω} [65].

The radius of a nucleation exclusion zone can be calculated on the basis of the following discussion, taking into account the charge transfer overpotential also. If there is a half-spherical nucleus on a flat electrode, the extent of the deviation in the shape of the equipotential surfaces which occurs around it depends on the crystallization overpotential, current density, resistivity of the solution, and radius of the nucleus r_N . If the distance from the flat part of the substrate surface to the equipotential surface which corresponds to the critical nucleation overpotential, η_n , is l , then this changes around defect to the extent kr_N , as is presented in Fig. 1.22.

Therefore, in this region the current lines deviate from straight lines towards the defect, thus causing an increase in the deposition

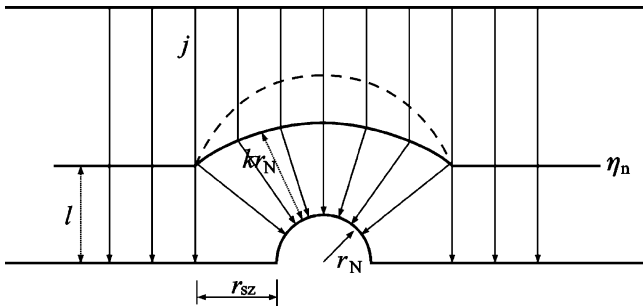


Fig. 1.22 A schematic representation of the deformation of the current field around a defect or a grain grown on a foreign substrate. For an explanation of the symbols see the text (Reprinted from [66] with permission from the Serbian Chemical Society and [67] with permission of Springer.)

rate, while in the surrounding region nucleation does not occur, i.e., a nucleation exclusion zone is formed. The voltage drop between the point from which the deviation occurs and the nucleus surface consists of the ohmic drop between these points and the charge transfer overpotential at the nucleus solution interface. The nucleation overpotential includes both the crystallization and charge transfer (deposition) overpotential:

$$\eta_n = \eta_{\text{cryst}} + \eta_d. \quad (1.69)$$

Hence, at the moment when kr_N become equal to l

$$kr_N j \rho = \eta_{\text{cr}}, \quad (1.70)$$

where j is the current density along the current lines and ρ is the electrolyte resistivity. Hence, when the ohmic drop between the deviation point and nucleus surface becomes equal to the crystallization overpotential, a new nucleation becomes possible on inert substrate assuming in both the cases the same charge transfer overpotential and the same value of the current density between the two symmetrical points on the anode and inert cathode surface and

between the same point on the anode and the point at the surface of the earlier formed nucleus.

The radius of the nucleation exclusion zone or screening zone, r_{sz} , corresponds to the distance between the edge of a nucleus and the first current line which does not deviate (when kr_N becomes equal to 1). Accordingly, nucleation will occur at distances from the edge of a nucleus equal or larger than r_{sz} , which can be calculated as

$$r_{sz} = r_N \left(\sqrt{2k + 1} - 1 \right). \quad (1.71)$$

If Eq. (1.70) is taken into account, one obtains

$$r_{sz} = r_N \left(\sqrt{\frac{2\eta_{cr}}{r_N \rho j} + 1} - 1 \right). \quad (1.72)$$

According to Eq. (1.72), a new nucleation is possible in the vicinity of a nucleus if $\eta_{cr} \rightarrow 0$ or $j \rightarrow \infty$ or $\rho \rightarrow \infty$.

During the cathodic process at low j/j_0 the crystallization overpotential is considerably high; with increasing j/j_0 , however, it decreases rapidly [68]. Hence, for $j_0 \rightarrow 0$, it follows that $r_{sz} \rightarrow 0$.

Electrodeposits of cadmium, copper, and nickel are shown in Figs. 1.23–1.25, respectively. In the cadmium deposition, boulders were formed by the independent growth of formed nuclei inside zones of zero nucleation. As a result of the high value of j_0 the deposition overpotential is low and the crystallization overpotential is relatively large and so the screening zone, according to Eq. (1.72), is relatively large. On the other hand, the nucleation rate is low. This results in the deposits shown in Fig. 1.23. These types of granular electrodeposits are mainly considered as disperse ones. In this chapter, only deposits based on dendritic and spongy growth will be treated as disperse ones in more details.

In the case of copper, a surface film is practically formed by a smaller quantity of electricity, as seen in Fig. 1.24, due to the lower exchange current density. The value of the deposition overpotential is larger than in the case of cadmium and the crystallization overpotential is lower, resulting in a decrease in the zero nucleation

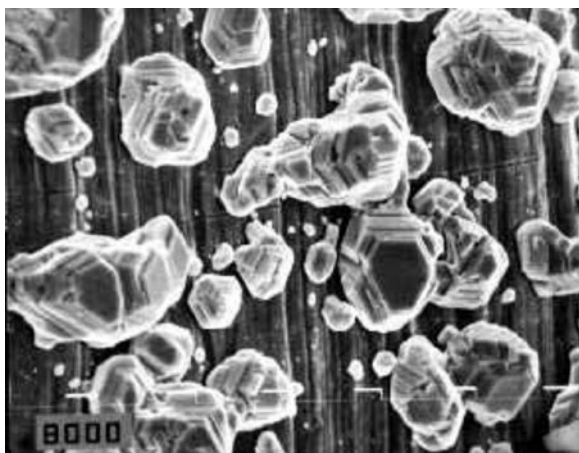


Fig. 1.23 Cadmium deposit on a copper substrate obtained at a current density of 1 mA cm^{-2} from 0.07 M CdSO_4 in $0.5 \text{ M H}_2\text{SO}_4$. Deposition overpotential: 15 mV . Deposition time $1,200 \text{ s}$. Magnification: $\times 2000$. (Reprinted from [33] with permission from the Serbian Chemical Society and [67] with permission of Springer.)

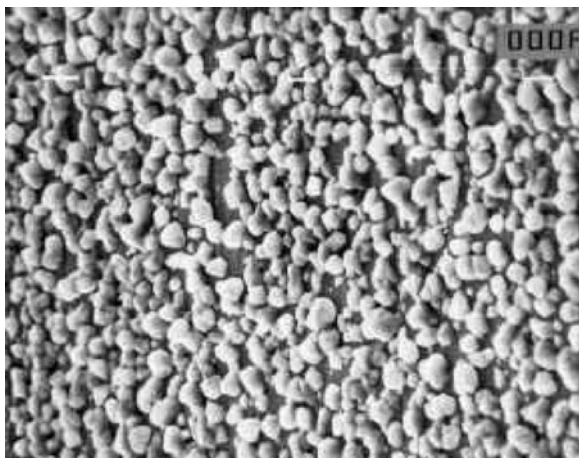


Fig. 1.24 SEM microphotograph of copper deposits on a silver substrate obtained at a current density of 1 mA cm^{-2} from 0.07 M CuSO_4 in $0.5 \text{ M H}_2\text{SO}_4$. Deposition overpotential: 60 mV . Deposition time 300 s . Magnification: $\times 5000$ (Reprinted from [33] with permission from the Serbian Chemical Society and [67] with permission of Springer.)

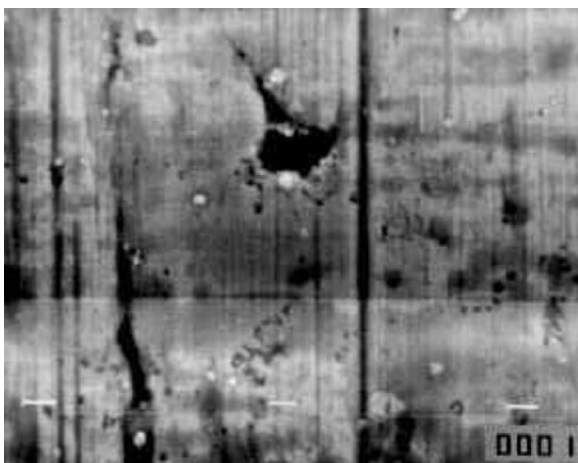


Fig. 1.25 SEM microphotograph of nickel deposits on a copper substrate obtained at a current density of 1 mA cm^{-2} from 0.07 M NiSO_4 in $0.5 \text{ M Na}_2\text{SO}_4 + 30 \text{ g/l H}_3\text{BO}_3$, $\text{pH} = 4$. Deposition overpotential: 715 mV . Deposition time: 120 s . Magnification: $\times 5000$ (Reprinted from [33] with permission from the Serbian Chemical Society and [67] with permission of Springer.)

zone radius, and hence a considerably larger nucleation rate. A further decrease in the exchange current density value, as in the case of Ni, leads to the situation shown in Fig. 1.25. A surface film is formed, but it is porous, probably due to hydrogen codeposition.

On the other hand, the classical expression for the steady-state nucleation rate, J , is given by [69–71]

$$J = K_1 \exp\left(-\frac{K_2}{\eta^2}\right), \quad (1.73)$$

where K_1 and K_2 are practically overpotential-independent constants. Equation (1.73) is valid for a number of systems regardless of the value of the exchange current density for the deposition process [69, 71]. At one and the same deposition current density, j , decreasing j_0 leads to an increasing nucleation rate and decreasing nucleation exclusion zones radii. Hence, the limiting case for nucleation

exclusion zones can be expected when $j/j_0 \rightarrow 0$, and the limiting case for active centers when $j/j_0 \rightarrow \infty$.

The saturation nucleus density, i.e., the exchange current density of the deposition process, strongly affects the morphology of metal deposits. At high exchange current densities, the radii of the screening zones are large and the saturation nucleus density is low. This permits the formation of large, well-defined crystal grains and granular growth of the deposit. At low exchange current densities, the screening zones radii are low, or equal to zero, the nucleation rate is large, and a thin surface film can be easily formed. The saturation nucleus density depends also on the deposition overpotential.

The nucleation law can be written as [72]

$$N = N_0[1 - \exp(-At)], \quad (1.74)$$

where

$$A = K_1 j_0 \exp\left(-\frac{K_2}{\eta^2}\right) \quad (1.75)$$

and N_0 is the saturation nucleus surface density (nuclei cm^{-2}), being dependent on the exchange current density of deposition process and the deposition overpotential.

The overpotential and the current density in activation-controlled deposition inside the Tafel region are related by

$$\eta = \frac{b_c}{2.3} \ln \frac{j}{j_0}. \quad (1.76)$$

Therefore, increasing b_c and decreasing j_0 leads to an increase in the deposition overpotential. According to Eq. (1.75), the value of A increases with increasing overpotential and decreases with decreasing exchange current density. It follows from all available data that the former effect is more pronounced resulting in deposits with a finer grain size with decreasing value of the exchange current density.

1.7 Spongy and Spongy–Dendritic Growth Initiation Inside Diffusion Layer of Microelectrodes

1.7.1 Spongy Deposits

According to Barton and Bockris [5], if the electrodeposition process on the microelectrode with

$$r \leq 55 \text{ } \mu\text{m} \quad (1.77)$$

is under complete diffusion control, a spherical diffusion layer, having a thickness equal to the radius of microelectrode is formed around it [5]. Equation (1.77) is always satisfied if

$$r \ll \delta. \quad (1.78)$$

Hence, it can be expected that the diffusion layer of hemispherical active particles on the inert substrate will not overlap if the distance between centers of the particles is larger than $4r$, as illustrated in Fig. 1.26a. The common diffusion layer of the macroelectrode will be formed at larger times.

In the case presented in Fig. 1.26b the diffusion layers of the microelectrodes are not formed and the diffusion layer of the macroelectrode

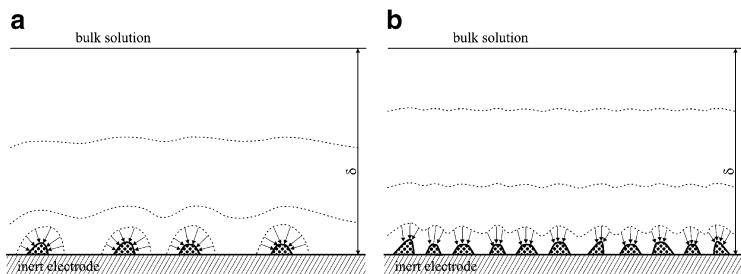


Fig. 1.26 Schematic presentation of formation of diffusion layer on the inert electrode covered with active grains. (a) The diffusion layers of macroelectrodes do not overlap and (b) the diffusion layers of the macroelectrodes overlap

is formed as on the massive electrode of active metal. Naturally, the initial electrodeposition on the grain from Fig. 1.26a will be performed in a spherical symmetry.

It follows from the previous discussion that this effect can be registered in the systems with the large j_0 values.

It follows from Eq. (1.1)

$$j = \frac{j_0(f_c - f_a)}{1 + \frac{j_0 f_c}{j_L}}, \quad (1.1)$$

that deposition in systems with low exchange current densities comes under full diffusion control at sufficiently large overpotentials. On the other hand, if:

$$\frac{j_0}{j_L} \gg 1 \quad (1.79)$$

deposition will be under complete diffusion control at all overpotentials if some other kind of control does not occur (e.g., for silver deposition on a well-defined silver crystal grains at a silver electrode at low overpotentials, two-dimensional nucleation is the rate-determining step) [73].

At low overpotentials a small number of nuclei are formed and they can grow independently. The limiting diffusion current density to the growing nucleus $j_{L,N}$ is given by

$$j_{L,N} = \frac{nFDC_0}{r_N}, \quad (1.80)$$

if

$$r_N < \delta, \quad (1.81)$$

where r_N is the radius of the nucleus. Hence, if $r_N \rightarrow 0$, the condition given by Eq. (1.79) is not satisfied and deposition is under activation or mixed control. Pure activation-controlled deposition is, thus, possible even at $j_0 \gg j_L$ on very small electrodes such as nuclei on an inert substrate.

An increase in r_N leads to a decrease of $j_{L,N}$, and, at sufficiently large r_N , the deposition comes under mixed activation–diffusion control, i.e., when

$$r_N > r_c, \quad (1.82)$$

where r_c is the radius of a growing nucleus where the process comes under mixed control [7, 74].

Under mixed control of the deposition, amplification of the surface irregularities on the growing nucleus occurs, leading to the formation of a spherical agglomerate of filaments. Thereby a spongy deposit is formed. The above reasoning is valid if spherical diffusion control can occur around growing grains, as in the case of cauliflower-like deposit growth. Assuming that around each grain with radius r_N , growing under spherical diffusion control, a diffusion layer of the same thickness is formed, then the initiation of spongy growth is possible if the number of nuclei per square centimeter, N , satisfies the condition

$$N \leq \frac{1}{(4r_c)^2}. \quad (1.83a)$$

Typical spongy electrodeposits are formed during zinc and cadmium electrodeposition at low overpotentials [7, 74]. Scanning electron microscopy images of zinc deposited at an overpotential of 20 mV onto a copper electrode from an alkaline zincate solution are shown in Fig. 1.27.

The increase in the number of nuclei formed with increasing deposition time can be seen in Fig. 1.27a, b, and a spongy deposit is formed as can be seen in Fig. 1.27b. The spongy growth takes place on a relatively small number of nuclei, as is shown in Fig. 1.27b, c.

The initiation of spongy growth at a fixed overpotential is possible if the condition $r_N > r_c$ (Eq. (1.82)) is satisfied, which is the case after some time. On the other hand, increasing the deposition time leads to the formation of a larger number of nuclei, and so the condition given by Eq. (1.83a) is not satisfied over a large part of the electrode surface. Regardless of this, the coverage of the electrode surface by spongy deposits increases with increasing deposition time up to full coverage, as can be seen in Fig. 1.27d.

Spongy growth can start on the growing nucleus if the conditions given by Eqs. (1.82) and (1.83a) are both satisfied simultaneously.

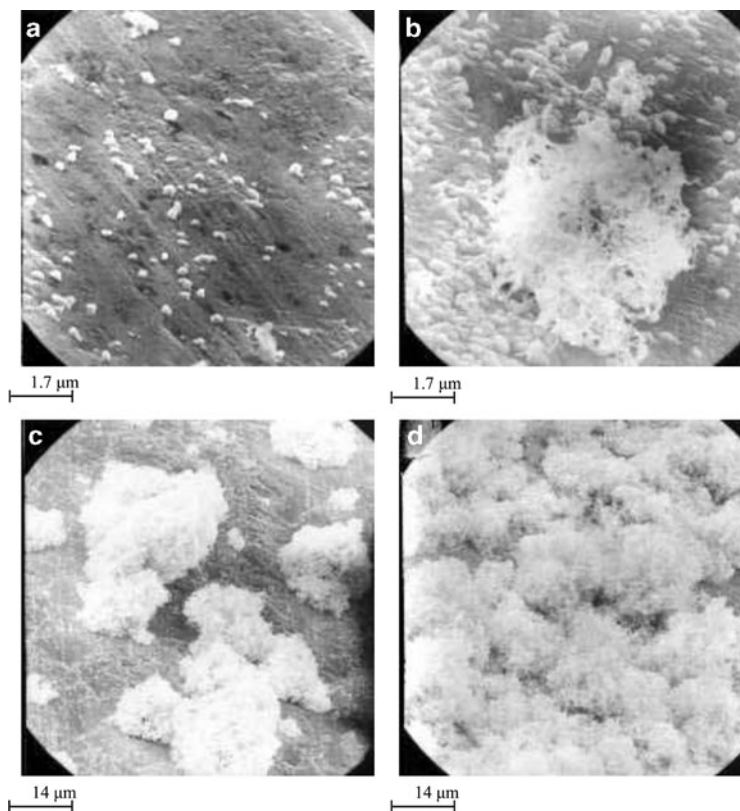


Fig. 1.27 Zinc deposits obtained by deposition at 20 mV from 0.1 M zincate and 1.0 M KOH solution. Deposition time (a) 10 min; (b) 20 min; (c) 30 min; and (d) 60 min (Reprinted from [7, 74, 75] with permission from Springer.)

In the first stage of deposition, the formation of nuclei having a regular crystal shape can be expected because the deposition is activation-controlled. After r_c is reached, the system comes under mixed control, producing polycrystalline grains like those shown in Fig. 1.28a, just as in the case of mixed control of copper deposition [12], Fig. 1.2c. In this situation, amplification of the surface irregularities on the growing grains occurs and spongy growth is initiated.

An ideal spongy nucleus obtained in a real system is shown in Fig. 1.28b which illustrates the above discussion. The agglomerate of

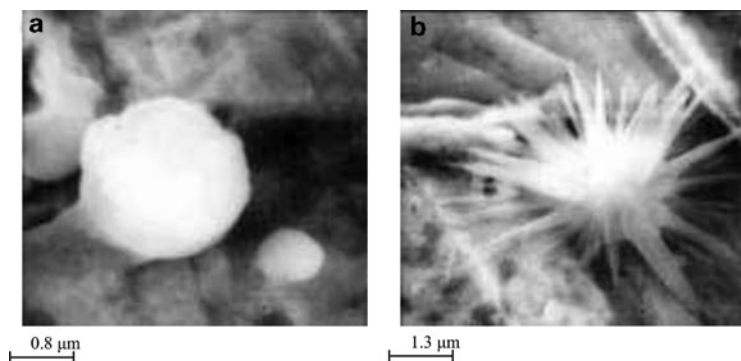


Fig. 1.28 Zinc deposits obtained by deposition at 35 mV from 0.1 M zincate solution in 1.0 M KOH solution. Deposition time (a) 7 min and (b) 15 min. The substrate is a copper plane electrode (Reprinted from [76] with permission from the Serbian Chemical Society and [7, 75] with permission from Springer.)

filaments in Fig. 1.27b is obviously formed by further growth of nuclei like that in Fig. 1.28b.

Hence, it can be concluded that at low overpotentials the initiation of spongy growth is due to the amplification of surface protrusions directly inside the spherical diffusion layer formed around each independently growing grain, as in the case of the formation of cauliflower-like deposits. The growth of protrusions in all directions is good proof that the initial stage of deposition on the grain is under spherical diffusion control, while further growth takes place in the diffusion layer of the macroelectrode. In less ideal situations, non-ideal spongy nuclei are formed, which, however, after further deposition result in a macroelectrode with the same appearance.

1.7.2 Spongy-Dendritic Deposits

The limiting diffusion current to the growing nucleus, $j_{L,N}$, can be related to j_L using Eqs. (1.5) and (1.80) by

$$j_{L,N} = \frac{\delta}{r_N} j_L, \quad (1.84)$$

where δ is the diffusion layer thickness of the macroelectrode of massive metal, and r_N is the radius of the growing nucleus. Equation (1.11) for the growing nucleus can be rewritten in the form

$$j_N = \frac{j_0 f_c}{1 + \frac{j_0 f_c}{j_L} \frac{r_N}{\delta}}, \quad (1.85)$$

where j_N is the current density to the growing nucleus. It is obvious from Eqs. (1.11) and (1.85) that deposition process on the macroelectrode can be under complete diffusion control if

$$\frac{j_0 f_c}{j_L} \gg 1 \quad (1.86)$$

and that at the same overpotential, process on the growing nucleus can be under pure activation control if

$$\frac{j_0 f_c}{j_L} \frac{r_N}{\delta} \ll 1 \quad (1.87)$$

or at

$$\frac{r_N}{\delta} \rightarrow 0. \quad (1.88)$$

Equations (1.87) and (1.88) are fulfilled in the initial stage of electrodeposition to the nuclei of metal formed on the inert substrate [77]. In this case the nuclei behave as microelectrodes, because of their complete independent growth well before the formation of the diffusion layer of the macroelectrode. The radius r_0 of the initial stable nucleus at overpotential η is given by [78]

$$r_0 = \frac{2\sigma V}{nF}, \quad (1.89)$$

where σ is the interfacial energy between metal and solution and V is the molar volume of the metal. The radius of the growing nucleus will vary with time according to [79]

$$r_N = r_0 + \frac{V}{nF} j_0 f_c t \quad (1.90)$$

or

$$r_N \approx \frac{V}{nF} j_0 f_c t \quad (1.91)$$

because r_0 is extremely low.

Obviously, Eqs. (1.85), (1.87), (1.90), and (1.91) are only the approximation on growth times, because the effect of surface energy has not been taken into consideration. At larger deposition times they are valid, because the surface energy term at higher value can be neglected [5].

An increase in r_N leads to a decrease of $j_{L,N}$, and at sufficiently large r_N deposition comes under mixed activation–diffusion control. It can be assumed that this happens at

$$j_N > v j_{L,N}, \quad (1.92)$$

where $0 < v < 1$. By combining Eqs. (1.85) and (1.92) one obtains

$$r_{c,N} \approx \frac{j_L v \delta}{j_0 f_c (1 - \kappa)}, \quad (1.93)$$

where $r_{c,N}$ is the radius of the growing nucleus when the process comes under mixed or spherical diffusion control. According to Barton and Bockris [5] the diffusion layer around such grain forms very fast. The further combination of Eqs. (1.91) and (1.93) gives the corresponding induction time, t_i , given by

$$t_i = \frac{j_L}{j_0^2} \frac{v F \delta}{V f_c^2 (1 - v)}. \quad (1.94)$$

For sufficiently high overpotentials Eqs. (1.93) and (1.94) can be rewritten in the forms [80]

$$r_{c,N} \approx \frac{j_L}{j_0} \frac{\delta}{4 f_c} \quad (1.95)$$

and

$$t_i = \frac{j_L}{j_0^2} \frac{nF\delta}{4Vf_c^2} \quad (1.96)$$

for $\nu = 0.2$.

At $r < r_{c,N}$ and $t < t_i$ the deposition on the growing grain is under activation control.

Hence, if $r_N > r_{c,N}$, the spherical diffusion layer around microelectrode can be formed. This is the condition for deposition in spherical diffusion control.

The nucleus of spongy deposit, i.e., hedgehog-like particle, appears when amplification of surface coarseness on the nucleus in spherical diffusion control starts growing. It was shown earlier [80] that this amplification is very fast so the induction time when growing nucleus enters mixed control can be taken also as induction time of spongy formation. It follows from Eqs. (1.95) and (1.96) that $r_{c,N}$ and t_i decrease with increasing overpotential.

On the other hand, it was also shown [74] that spongy deposit can be formed only if around each grain with radius $r_{c,N}$, growing under spherical diffusion control, a diffusion layer of the same thickness is formed, as illustrated earlier. This condition is fulfilled if

$$N \leq \frac{1}{(4r_{c,N})^2}, \quad (1.83b)$$

where N is the number of grain per square centimeter of the macroelectrode. Hence, deposition in spherical diffusion control on the growing grain is possible if both Eqs. (1.93) and (1.83b) are satisfied in the same time the nucleation law can be written in the form [72]

$$N = N_0 [1 - e^{-At}], \quad (1.74)$$

where

$$A = K_1 j_0 e^{-\frac{K_2}{\eta^2}}. \quad (1.75)$$

N_0 is the maximum number of active sites for selected value of overpotential and K_1 and K_2 are constants.

Spongy deposits formation is possible if

$$N_0 [1 - e^{-At_i}] < \frac{1}{4r_{c,N}^2} \quad (1.97)$$

and

$$At_i \approx 0 \quad (1.98)$$

which happens at sufficiently high overpotentials where $K_2/\eta^2 \rightarrow 0$, $A \rightarrow K_1 j_0$ and $t_i \rightarrow 0$. Hence, the spongy deposit formation at high overpotentials starts at very low deposition times, when the spherical diffusion layer formed around grains do not overlap. The critical overpotential of spongy formation can be obtained by substitution of $r_{c,N}$ from Eq. (1.95) and t_i from Eq. (1.96) in Eq. (1.97) and further calculation. if this overpotential is larger than critical one for instantaneous dendritic growth the dendrite spongy nuclei can be formed over inert substrate.

The experimental verification of the above discussion is given by the consideration of the morphology of electrodeposited silver from 0.50 M AgNO_3 in 0.20 M HNO_3 on the graphite electrode at different overpotentials of deposition and with different deposition times [81]. In Fig. 1.29 the deposit obtained at an overpotential of 100 mV during 180 s is shown.

As expected, the boulders are obtained. In Fig. 1.30, the deposits obtained at 200 mV during 1 and 10 s are presented. At 1 s, the boulders are formed, but at 10 s the needle-like deposit is obtained. This means that the spherical diffusion layer around the growing grains is not formed before the formation of the diffusion layer of the macroelectrode. The electrodeposition inside the diffusion layer of the macroelectrode is confirmed by the growth of needles towards the bulk of solution.

At an overpotential of 300 mV, the conditions of the spherical diffusion control around the growing grains are fulfilled and dendritic-spongy deposit is formed, as can be seen from Fig. 1.31.

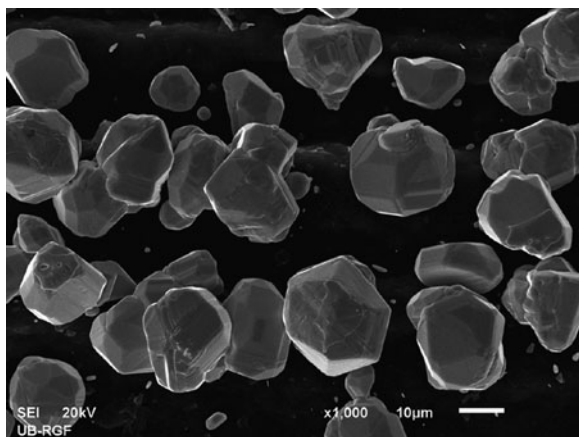


Fig. 1.29 Silver deposit obtained at an overpotential of 100 mV with electrolysis time of 180 s

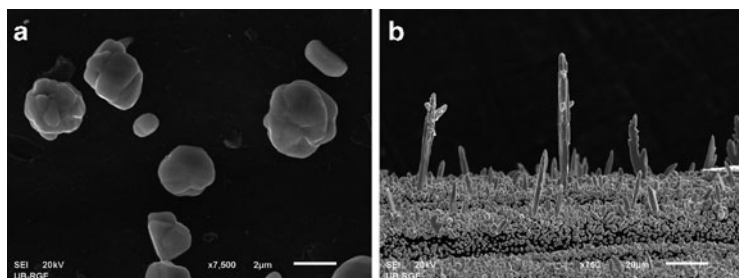


Fig. 1.30 Silver deposit obtained at an overpotential of 200 mV. Deposition time (a) 1 s and (b) 10 s

The growth of dendrites in all directions means that there is a spherical control to the growing grains in the initial stage of the electrodeposition.

Finally, the fact that $r_{c,N}$ and t_i (Eqs. (1.95) and (1.96)) decrease with the increasing overpotential can be verified by Figs. 1.31 and 1.32.

It is obvious that the semiquantitative agreement between the theory and experiments is fair. Besides, the deposits from Figs. 1.31 and 1.32 are similar to those from Fig. 1.29. Unfortunately, the ideal spongy–dendritic

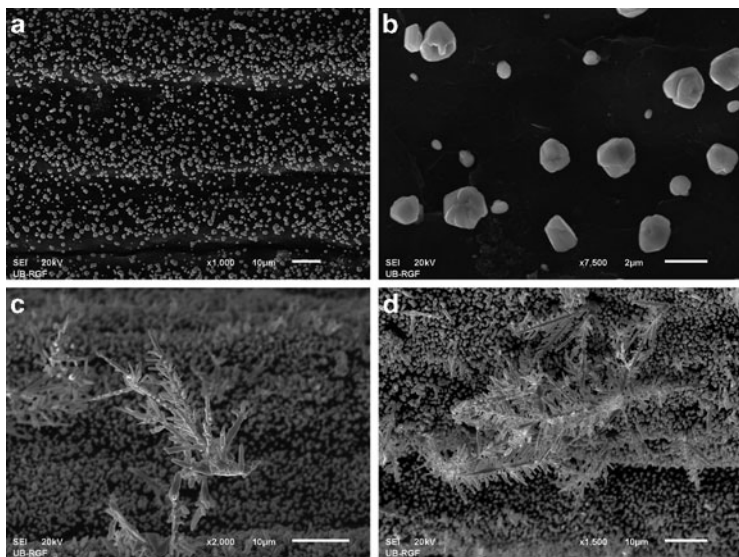


Fig. 1.31 Silver deposits obtained at an overpotential of 300 mV (a) 1 s; (b) 1 s; (c) 3 s, and (d) 5 s

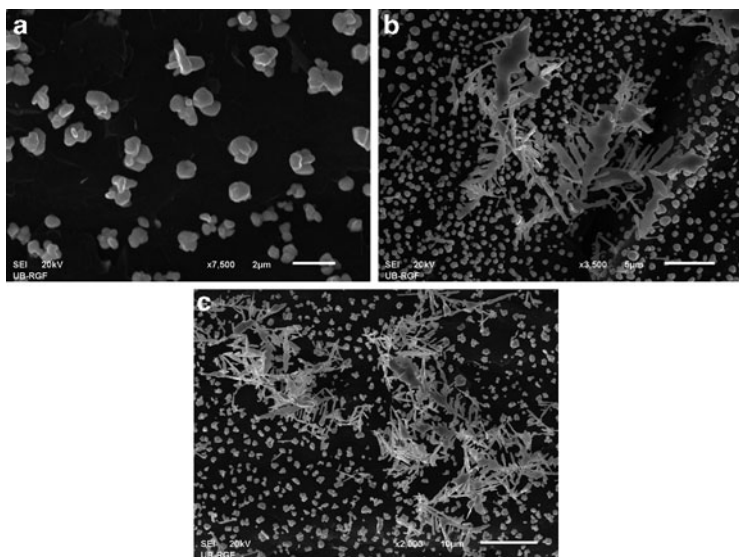


Fig. 1.32 Silver deposits obtained at an overpotential of 700 mV (a) 0.15 s; (b) 0.30 s; and (c) 0.5 s

nucleus similar to the one from Fig. 1.30 has not been formed so far; it will probably be formed in the future investigations.

1.8 Conclusions

The formation of disperse metal electrodeposits is discussed by the consideration of corresponding physical and mathematical models. It is shown that the mechanisms of formation of all different forms can be elucidated by the use of conclusions of a few classic works in the field of metal electrodeposition making a general theory of disperse metal electrodeposits formation.

The appearance of different forms of disperse metal electrodeposits is correlated with the properties of electrodeposited metal and deposition conditions. In this way, the theoretical basis of powdered electrodeposits formation and inert electrodes activation is formed.

Acknowledgments This chapter is based on a few classical studies and a research in the field of metal electrodeposition performed at the Department of Physical Chemistry and Electrochemistry at the Faculty of technology and Metallurgy and Institute of Electrochemistry, ICTM, University of Belgrade, Serbia. We would like to acknowledge all colleagues and students who participated in it.

The work was supported by the Ministry of Education and Science of the Republic of Serbia under the research project: “Electrochemical synthesis and characterization of nanostructured functional materials for application in new technologies” (No. 172046).

References

1. Popov KI, Živković PM, Nikolić ND (2010) The effect of morphology of activated electrodes on their electrochemical activity. In: Djokić SS (ed) *Electrodeposition: theory and practice. Modern aspects of electrochemistry*, vol. 48. Springer, Berlin, pp 163–213, 165
2. Bockris JO'M, Reddy AKN, Gamboa-Aldeco M (2000) *Modern electrochemistry 2A*, 2nd edn. Kluwer Academic/Plenum, New York, p 1248
3. Diggle JW, Despić AR, Bockris JO'M (1969) *J Electrochem Soc* 116:1503
4. Popov KI, Djokić SS, Grgur BN (2002) *Fundamental aspects of electrometallurgy*, chap 3. Kluwer Academic/Plenum, New York, p 14

5. Barton JL, Bockris JO'M (1962) *Proc Roy Soc A* 268:485
6. Popov KI, Živković PM, Grgur BN (2007) *Electrochim Acta* 52:4696
7. Popov KI, Krstajić NV, Čekerevac MI (1996) The mechanism of formation of coarse and disperse electrodeposits. In: White RE, Conway BE, Bockris JO'M (eds) *Modern aspects of electrochemistry*, vol 30. Plenum, New York, pp 261–312, 262
8. Despić AR, Diggle JW, Bockris JO'M (1969) *J Electrochem Soc* 116:507
9. Gilleadi E (1993) *Electrode kinetics*. VCH, New York, p 443
10. Popov KI, Djokić SS, Grgur BN (2002) *Fundamental aspects of electrometallurgy*, chap 3. Kluwer Academic/Plenum, New York, p 56
11. Damjanović A (1965) *Plating* 52:1017
12. Popov KI, Pavlović MG, Pavlović LjJ, Čekerevac MI, Remović GŽ (1988) *Surf Coat Technol* 34:355
13. Popov KI, Grgur BN, Pavlović MG, Radmilović V (1993) *J Serb Chem Soc* 58:1055
14. Popov KI, Radmilović V, Grgur BN, Pavlović MG (1994) *J Serb Chem Soc* 59:47
15. Popov KI, Djokić SS, Grgur BN (2002) *Fundamental aspects of electrometallurgy*, chap 3. Kluwer Academic/Plenum, New York, p 78
16. Despić AR, Popov KI (1972) Transport controlled deposition and dissolution of metals. In: Conway BE, Bockris JO'M (eds) *Modern aspects of electrochemistry*, vol 7. Plenum, New York, pp 199–313, 203, 220
17. Popov KI, Krstajić NV, Čekerevac MI (1996) The mechanism of formation of coarse and disperse electrodeposits. In: White RE, Conway BE, Bockris JO'M (eds) *Modern aspects of electrochemistry*, vol 30. Plenum, New York, pp 261–312, 294
18. Wranglen G (1960) *Electrochim Acta* 2:130
19. Bechtoldt CJ, Ogburn F, Smith J (1968) *J Electrochem Soc* 115:813
20. Faust JW, John HF (1963) *J Electrochem Soc* 110:463
21. Faust JW, John HF (1961) *J Electrochem Soc* 108:855
22. Justinijanović IN, Despić AR (1973) *Electrochim Acta* 18:709
23. Newman JS (1973) *Electrochemical systems*. Prentice-Hall, Englewood Cliffs, NJ, p 177
24. Popov KI, Maksimović MD, Trnjavčev JD, Pavlović MG (1981) *J Appl Electrochem* 11:239
25. Popov KI, Živković PM, Nikolić ND (2010) The effect of morphology of activated electrodes on their electrochemical activity. In: Djokić SS (ed) *Electrodeposition: theory and practice. Modern aspects of electrochemistry series*, vol 48. Springer, Berlin, pp 163–213, 171
26. Scharifker B, Hills G (1983) *Electrochim Acta* 28:879
27. Popov KI, Živković PM, Krstić SB, Nikolić ND (2009) *Electrochim Acta* 54:2924
28. Bockris JO'M, Reddy AKN, Gamboa-Aldeco M (2000) *Modern electrochemistry 2 A*, 2nd edn. Kluwer Academic/Plenum, New York, p 1107
29. Popov KI, Djokić SS, Grgur BN (2002) *Fundamental aspects of electrometallurgy*, chap 3. Kluwer Academic/Plenum, New York, pp 87, 88

30. Price PB, Vermilyea DA (1958) *J Chem Phys* 28:720
31. Lorenz W (1954) *Z Electrochem* 58:912
32. Mattsson BE, Bockris JO'M (1959) *Trans Faraday Soc* 55:1586
33. Popov KI, Grgur BN, Stojilković ER, Pavlović MG, Nikolić ND (1997) *J Serb Chem Soc* 62:433
34. Meibhur S, Yeager E, Kozawa A, Hovorka F (1963) *J Electrochem Soc* 110:190
35. Popov KI, Pavlović MG, Stojilković ER, Stevanović ZŽ (1997) *Hydrometallurgy* 46:321
36. Popov KI, Živković PM, Nikolić ND (2010) The effect of morphology of activated electrodes on their electrochemical activity. In: Djokić SS (ed) *Electrodeposition: theory and practice. Modern aspects of electrochemistry*, vol 48. Springer, Berlin, pp 163–213, 190
37. Popov KI, Radmilović V, Grgur BN, Pavlović MG (1994) *J Serb Chem Soc* 59:119
38. Popov KI, Čekerevac MI (1989) *Surf Coat Technol* 37:435
39. Popov KI, Djokić SS, Grgur BN (2002) *Fundamental aspects of electrometallurgy*, chap 2. Kluwer Academic/Plenum, New York, p 24
40. Popov KI, Pavlović MG (1993) Electrodeposition of metal powders with controlled grain size and morphology. In: White RE, Bockris JO'M, Conway BE (eds) *Modern aspects of electrochemistry*, vol 24. Plenum, New York, pp 299–391, 300
41. Calusaru A (1979) *Electrodeposition of metal powders. Material science monography*, vol 3. Elsevier, Amsterdam
42. Popov KI, Krstajić NV, Pantelić RM, Popov SR (1985) *Surf Technol* 26:177
43. Popov KI, Pavlović MG, Jovičević JN (1989) *Hydrometallurgy* 23:127
44. Pangarov NA (1967) *Phys Stat Sol* 20:371
45. Nikolić ND, Popov KI, Pavlović LjJ, Pavlović MG (2006) *J Electroanal Chem* 588:88
46. Nikolić ND, Popov KI (2010) Hydrogen co-deposition effects on the structure of electrodeposited copper. In: Djokić SS (ed) *Electrodeposition: theory and practice. Modern aspects of electrochemistry*, vol 48. Springer, Berlin, pp 1–70
47. Nikolić ND, Popov KI, Pavlović LjJ, Pavlović MG (2006) *Surf Coat Technol* 201:560
48. Ibl N (1961) *Chemie Ing Techn* 33:69
49. Ibl N (1963) *Chemie Ing Techn* 35:353
50. Jensen LJ, Hoogland JG (1970) *Electrochim Acta* 15:1013
51. Bockris JO'M, Reddy AKN, Gamboa M (2000) *Aldeco, Modern electrochemistry 2A, Fundamentals of electroics*, 2nd edn. Kluwer Academic/Plenum, New York
52. Nikolić ND, Popov KI, Pavlović LjJ, Pavlović MG (2007) *J Solid State Electrochem* 11:667
53. Nikolić ND, Pavlović LjJ, Pavlović MG, Popov KI (2007) *Electrochim Acta* 52:8096
54. Nikolić ND, Popov KI, Pavlović LjJ, Pavlović MG (2007) *Sensors* 7:1

55. Nikolić ND, Pavlović LjJ, Krstić SB, Pavlović MG, Popov KI (2008) *Chem Eng Sci* 63:2824
56. Nikolić ND, Branković G, Pavlović MG, Popov KI (2008) *J Electroanal Chem* 621:13
57. Nikolić ND, Pavlović LjJ, Branković G, Pavlović MG, Popov KI (2008) *J Serb Chem Soc* 73:753
58. Nikolić ND, Pavlović LjJ, Pavlović MG, Popov KI (2007) *J Serb Chem Soc* 72:1369
59. Nikolić ND, Branković G, Pavlović MG, Popov KI (2009) *Electrochem Commun* 11:421
60. Nikolić ND, Branković G, Maksimović VM, Pavlović MG, Popov KI (2010) *J Solid State Electrochem* 14:331
61. Nikolić ND, Branković G, Maksimović VM, Pavlović MG, Popov KI (2009) *J Electroanal Chem* 635:111
62. Popov KI, Nikolić ND, Živković PM, Branković G (2010) *Electrochim Acta* 55:1919
63. Popov KI, Živković PM, Nikolić ND (2010) The effect of morphology of activated electrodes on their electrochemical activity. In: Djokić SS (ed) *Electrodeposition: theory and practice*, vol 48, Modern aspects of electrochemistry. Springer, Berlin, pp 163–213
64. Jović VD, Maksimović V, Pavlović MG, Popov KI (2006) *J Solid State Electrochem* 10:373
65. Markov I, Boynov A, Toshev S (1973) *Electrochim Acta* 18:377
66. Štrbac S, Rakočević Z, Popov KI, Pavlović MG, Petrović R (1999) *J Serb Chem Soc* 64:483
67. Popov KI, Djokić SS, Grgur BN (2002) *Fundamental aspects of electrometallurgy*, chap 3. Kluwer Academic/Plenum, New York, p 30
68. Klapka V (1970) *Collection Czechoslov Chem Commun* 35:899
69. Gutzov I (1964) *Izv Inst Fiz Chim Bulgar Acad Nauk* 4:69
70. Erdey-Grúz T, Volmer Z (1931) *Z Phys Chem* 157A:165 (in German)
71. Fetter K (1967) *Electrochemical kinetics*. Khimiya, Moscow (in Russian)
72. Fleischmann M, Thirsk HR (1959) *Electrochim Acta* 1:146
73. Popov KI, Krstajić NV, Jerotijević ZĐ, Marinković SR (1985) *Surf Technol* 26:185
74. Popov KI, Krstajić NV (1983) *J Appl Electrochem* 13:775
75. Popov KI, Djokić SS, Grgur BN (2002) *Fundamental aspects of electrometallurgy*, chap 3. Kluwer Academic/Plenum, New York, p 72
76. Popov KI, Krstajić NV, Simićić MV, Bibić NM (1992) *J Serb Chem Soc* 57:927
77. Popov KI, Krstajić NV, Popov SR, Čekerevac MI (1986) *J Appl Electrochem* 14:771
78. Toshev S, Markov I (1967) *Electrochim Acta* 12:489
79. Bockris JO'M, Nagy Z, Dražić D (1973) *J Electrochem Soc* 120:30
80. Popov KI, Krstajić NV, Popov SR (1985) *J Appl Electrochem* 15:151
81. Popov KI, Nikolić ND, Živković PM (2012) *Int J Electrochem Sci* 7:686